

Review

# A Concise Review on Materials for Injection Moulds and Their Conventional and Non-Conventional Machining Processes

André F. V. Pedroso <sup>1</sup>, Naiara P. V. Sebbe <sup>1</sup>, Francisco J. G. Silva <sup>1,2,\*</sup>, Raul D. S. G. Campilho <sup>1,2</sup>, Rita C. M. Sales-Contini <sup>1,3</sup>, Rúben D. F. S. Costa <sup>2,4</sup>, Marta L. S. Barbosa <sup>4</sup> and Francisca R. Nogueira <sup>1</sup>

<sup>1</sup> CIDEM, ISEP, Polytechnic of Porto, Rua Dr. António Bernardino de Almeida, 4249-015 Porto, Portugal; afvpe@isep.ipp.pt (A.F.V.P.); napvs@isep.ipp.pt (N.P.V.S.); rds@isep.ipp.pt (R.D.S.G.C.); rcmcs@isep.ipp.pt or rita.sales@fatec.sp.gov.br (R.C.M.S.-C.); frno@isep.ipp.pt (F.R.N.)

<sup>2</sup> LAETA-INEGI, Associate Laboratory for Energy, Transports and Aerospace, Rua Dr. Roberto Frias 400, 4200-465 Porto, Portugal; rdcosta@inegi.up.pt

<sup>3</sup> Technological College of São José dos Campos, Centro Paula Souza, Avenida Cesare Mansueto Giulio Lattes, 1350 Distrito Eugênio de Melo, São José dos Campos 12247-014, Brazil

<sup>4</sup> Department of Mechanical Engineering, Faculty of Engineering, University of Porto, Rua Dr. Roberto Frias 400, 4200-465 Porto, Portugal; martabarbosa8c@gmail.com

\* Correspondence: fgs@isep.ipp.pt; Tel.: +351-228-340-500

**Abstract:** Injection moulds are crucial to produce plastic and lightweight metal components. One primary associated challenge is that these may suffer from different types of failures, such as wear and/or cracking, due to the extreme temperatures ( $T$ ), thermal cycles, and pressures involved in the production process. According to the intended geometry and respective needs, mould manufacturing can be performed with conventional or non-conventional processes. This work focuses on three foremost alloys: AMPCO<sup>®</sup> (CuBe alloy), INVAR-36<sup>®</sup> (Fe-Ni alloys, Fe-Ni36), and heat-treated (HT) steels. An insight into the manufacturing processes' limitations of these kinds of materials will be made, and solutions for more effective machining will be presented by reviewing other published works from the last decade. The main objective is to provide a concise and comprehensive review of the most recent investigations of these alloys' manufacturing processes and present the machinability challenges from other authors, discovering the prospects for future work and contributing to the endeavours of the injection mould industry. This review highlighted the imperative for more extensive research and development in targeted domains.

**Keywords:** traditional manufacturing; unconventional machining; plastic injection moulding; high-pressure injection moulding; copper alloys; iron–nickel alloys; heat-treated steels



**Citation:** Pedroso, A.F.V.; Sebbe, N.P.V.; Silva, F.J.G.; Campilho, R.D.S.G.; Sales-Contini, R.C.M.; Costa, R.D.F.S.; Barbosa, M.L.S.; Nogueira, F.R. A Concise Review on Materials for Injection Moulds and Their Conventional and Non-Conventional Machining Processes. *Machines* **2024**, *12*, 255. <https://doi.org/10.3390/machines12040255>

Academic Editors: Katarzyna Antosz, Vitalii Ivanov and Ivan Pavlenko

Received: 18 March 2024

Revised: 29 March 2024

Accepted: 9 April 2024

Published: 11 April 2024



**Copyright:** © 2024 by the authors. Licensee MDPI, Basel, Switzerland. This article is an open access article distributed under the terms and conditions of the Creative Commons Attribution (CC BY) license (<https://creativecommons.org/licenses/by/4.0/>).

## 1. Introduction

Injection moulds are used in the manufacturing process of a wide variety of products, and these can be made from different materials with unique properties for given applications. Injection moulding requires a substantial amount of material to fabricate them, resulting in expensive mould costs and the installation of supplementary equipment. It is a vital process in polymer processing [1] that produces rework-free moulded parts from raw materials. The high flexibility associated with injection moulding elevates the process across various industries [2]. Quality criteria such as dimensional accuracy, surface impression, and the minimum achievable cycle time are essential considerations [3,4]. Numerous examples of injection mould products include short-glass-fibre composites, thermoplastic and thermosetting polymers, and standard plastic [5]. The high-pressure injection moulding (HPIM) industry is rapidly expanding due to the extensive use of these products. Fe alloys are more commonly used to produce injection moulds since mechanical strength, corrosion resistance, hardness, wear resistance, and fatigue resistance are guaranteed at lower costs [6–8]. The present review will focus on three primary alloys used in HPIM.

CuBe or AMPCO<sup>®</sup> alloys are popular for plastic injection moulds due to their excellent thermal conductivity ( $k$ ), allowing for fast and efficient mould cooling. Additionally, this alloy is highly resistant to corrosion and wear, making it an ideal material for high- $T$  and high-pressure moulding applications; Fe-Ni36 or INVAR-36<sup>®</sup> is commonly used in injection moulds. These materials are known for their low thermal expansion coefficient ( $\alpha$ ), meaning they maintain their dimensional stability even when exposed to  $T$  changes, and heat-treated (HT) steels are ideal for high-volume moulding applications where durability is critical [9,10].

### 1.1. Copper–Beryllium Alloys (AMPCO<sup>®</sup>)

The incorporation of Cu [11,12] in the HPIM process, especially in Polymer Injection Moulding (PIM), enhances (1) elevated  $k$ , (2) corrosion and wear resistance, (3) dimensional stability, (4) electrical resistivity ( $\rho_R$ ), and (5) substantial mechanical strength [13]. Cu alloys are extensively utilized across diverse industries due to their exceptional properties. Nonetheless, the surface quality of these materials holds paramount importance in ensuring optimal performance in moulds. Consequently, various cleaning processes enhance surface quality, including mechanical, chemical, chemical–mechanical, and electrochemical polishing [14]. During manufacturing, lubricating oils, drawing compounds, dirt, oxides, and metallic particles can accumulate, and these impurities must be eliminated to ensure quality. Chemical and chemical–mechanical polishing methods can yield finishes closely resembling those achieved through electropolishing, a technique known for creating smoother and brighter surfaces.

Moreover, electropolishing offers a more straightforward process that can effectively be applied to larger surface areas [15,16]. On the contrary, Be [17] is acknowledged for its inherent hardness and granular state, requiring powder metallurgy technology. Additionally, Be and its compounds are toxic, which can incur high costs and complexity in manufacturing and repair/service [18–21]. This inherent characteristic poses challenges in attaining polished and flawless surfaces due to the abrasive nature of the hard particles, thereby exacerbating tool wear during the machining of an injection moulding insert of a Cu-Be [22] alloy by amplifying the costs and intricacy associated with manufacturing and repair/service procedures [19]. Figure 1 depicts a binary phase diagram of CuBe alloys.

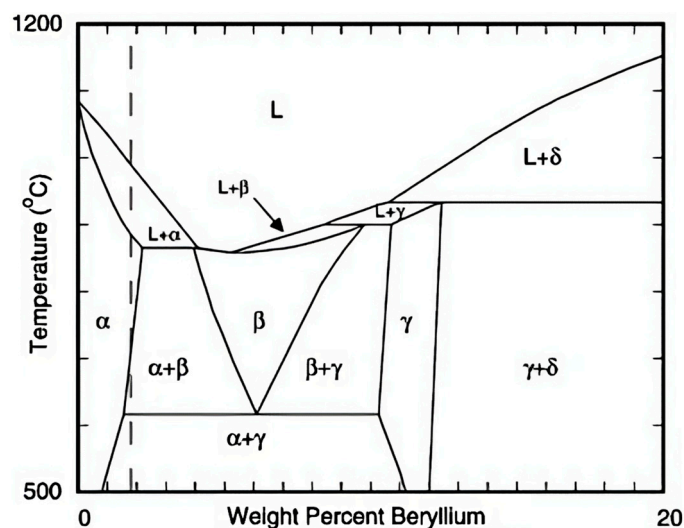


**Figure 1.** The binary CuBe phase diagram. The composition range of interest typically contains approximately 1.8 weight percentage (wt%) of Be, denoted by the vertical dashed line [23].

CuBe alloys, such as those found in AMPCO<sup>®</sup> alloys, are often employed for PIM [24]. Zhong et al. [25] compared a rapidly solidified Al alloy, CuBe C17200 alloy, according to the ASTM B 194-15 [26] standard, and Al-6061 alloy regarding their wear rates, hardness, and suitability as materials for mould inserts. Among the materials examined for mould

inserts, the CuBe alloy exhibited the highest hardness and the lowest wear rate, whereas the Al-6061 alloy was the worst material. Cu alloying with Be enhances its mechanical properties while significantly decreasing  $k$  [27,28]. AMPCO<sup>®</sup> variants' incorporation into PIM tools can enhance the efficiency and quality of the moulding process [29]. It merges the characteristics of Cu [11,12] and Be [17] to create a sturdy alloy with improved resistance to wear due to high hardness and excellent seizing and galling resistance. These characteristics make this alloy an excellent option for bearing and bushing applications [30,31] and from aerospace to automotive and nuclear sectors, as presented in Table 1 [32].

**Table 1.** Industry applications and characteristics of AMPCO<sup>®</sup> alloys.

Alloy	Industry Applications	Characteristics
AMPCO <sup>®</sup> 83 [14,33,34]	Construction of chill plates, Inserts in moulds, Cooling pins, Neck rings or bottom plates for blow moulds of plastic bottles, Resistance welding, Steel mills, Flash butt welding and butt welding, Parts for electrical components.	High levels of hardness, Excellent corrosion resistance, Good machinability, Easy to polish, Weld repairable, Good electric or thermal conductivity.
AMPCO <sup>®</sup> 88	Flash welding dies, Welding wheels, Electrodes for mesh welding, Damper ring segments, Damper rings for generators, Parts for injection moulding of plastic, Die-casting and resistance welding components.	Good machinability, Extremely resistant to wear and corrosion, Superior thermal conductivity.
AMPCO <sup>®</sup> 89	Welding wheels, Flash welding dies, Plunger tips in Al die-cast, Casting machines, Components in moulds for PIM.	Good machinability, Higher electrical conductivity, Heat transfer properties, Extremely resistant to wear and corrosion, Superior thermal conductivity.
AMPCO <sup>®</sup> 91	Spot welding electrodes, Electrodes for mesh welding, Electrode holders, Seam welding discs for stainless steel, Flash welding dies, Plunger tips for Al high-pressure die-casting machines.	Extremely resistant to wear and corrosion, High thermal conductivity (desirable).

As a result, several investigations have been carried out into processing these alloys for injection moulding applications, focusing on the electrical discharge machining of Cu-based alloys. This method has proven highly effective in producing mould cavities. High-reliability engineered materials, specifically CuBe alloys, have gained widespread utilization in numerous engineering domains. Due to the high hardness of Be particles and  $T$  fatigue strength, machining challenges, such as tool wear (TW), built-up edge (BUE), where material adhesion to tool surfaces can cause rapid tool deterioration [14,34], and the micro-tearing of the grain lattice may arise, when creating smooth surfaces on AMPCO<sup>®</sup> alloys using CM methods [35,36]. Research has focused on overcoming these challenges, including electrical discharge machining (EDM) [37] and diamond-like-coated tools. Table 2 presents some AMPCO<sup>®</sup> alloys' chemical compositions, which can differ from the contents established by the ASTM B 194-15 [26] standard since it is heavily commercial branded material. Enterprises tend to compete with their counterparts who have specific know-how, thus adding more wt% of certain elements to enhance performance. Table 3 presents some critical physical, mechanical, and thermodynamical properties of AMPCO<sup>®</sup> and CuBe C17200 alloys.

**Table 2.** Chemical composition of some AMPCO<sup>®</sup> alloys.

	wt%							
	Cu	Be	Co + Ni	Co	Ni	Si	Al	Others
AMPCO <sup>®</sup> 83 [14,34]	Bal.	2.0	0.5	-	-	-	-	≤0.5
AMPCO <sup>®</sup> 88 [38]	Bal.	0.5	2.5	-	-	-	-	≤0.5
AMPCO <sup>®</sup> 89 [38]	Bal.	0.4	-	0.3 max.	2.8	-	-	≤0.4
AMPCO <sup>®</sup> 91 [38]	Bal.	0.5	-	2.4	-	-	-	≤0.5
CuBe C17200 [26]	Bal.	1.9	-	0.2	-	-	-	-
CuBe C17200 [39]	Bal.	1.8–2.0	≥0.2	-	-	≤0.2	≤0.2	-

Bal.—balance.

**Table 3.** Physical, mechanical, and thermodynamic properties of some AMPCO<sup>®</sup> alloys.

Property	AMPCO <sup>®</sup> Alloys					Units
	83 [14,34]	88	89	91		
				Ø ≤ 35 mm	Ø ≥ 35 mm	
E	128	130	135	130	130	GPa
$\nu$	-	-	-	-	-	[-]
$\sigma_u$	1140	890	740	900	723	MPa
$\sigma_y$	1000	680	680	550	517	MPa
HV	376	277	235	262	255	HV
$\epsilon_u$	5	14	12	10	17	%
$\rho$	8260	8750	8800		8750	kg/m <sup>3</sup>
$\alpha$	17.5	17.0	17.2		17.0	10 <sup>-6</sup> /K
k (@100 °C)	130	230	300		208	W/m·K

E—Young's Modulus, HV—Vickers' hardness,  $\epsilon_u$ —strain at fracture,  $\rho$ —volumetric mass density,  $\sigma_u$ —tensile strength,  $\sigma_y$ —yield strength.

### 1.2. Iron–Nickel (INVAR-36<sup>®</sup>)

INVAR-36<sup>®</sup> is a ferromagnetic Ni alloy classified in the Fe–Ni [40] and Fe-based superalloy series. Shallow  $\alpha$  values characterize it over a wide range of  $T$  of  $20 < T < 200$  °C [41], known as INVAR behaviour. Ruled by the ASTM F 1684-06 (2016) [42] standard, this alloy has emerged as a crucial material in advancing science and technology, particularly for precision measurements [43,44]. Due to the unique properties of Fe–Ni alloys with a Face-Centred Cubic (FCC) structure and a Ni concentration of approximately wt% = 36% (Figure 2), these materials exhibit the most excellent INVAR behaviour [44,45], excellent for dimensional stability applications such as (1) the Aerospace industry, (2) Appliance and heater thermostats, (3) Automotive control devices, (4) Bimetals for circuit breakers, (5) Composite layup moulds, (6) Gauge tubes, (7) Heating and air conditioning, (8) Metrology devices, (9) Motor controls, (10) Optical mounting and components, (11) Orbiting satellites, (12) Precision measuring instruments/tools, (13) Ring laser gyroscopes, (14) Shadow masks to produce Organic Light-Emitting Diodes (OLEDs), and (15) Time-keeping devices.

However, its low hardness limits its use in tribological applications, such as manufacturing bulky composite tooling for the aerospace [46] and automotive industries. The production of structural components from Fe–Ni alloys maintains its popularity due to their excellent resistance to chemical and environmental corrosion [47,48], fatigue resistance, mechanical properties in low  $T$  environments, reasonable ductility, and toughness. The hot ductility of the base metal Fe–Ni36 can be improved by increasing the strain rate ( $\dot{\epsilon}$ ), in the range of  $0.001 < \dot{\epsilon} < 1$  Hz or by the influence of dynamic recrystallization at high  $T$  [49,50]. Tables 4 and 5 present some important physical, mechanical, and thermodynamical properties of INVAR-36<sup>®</sup> and the typical chemical composition according to some authors, respectively.

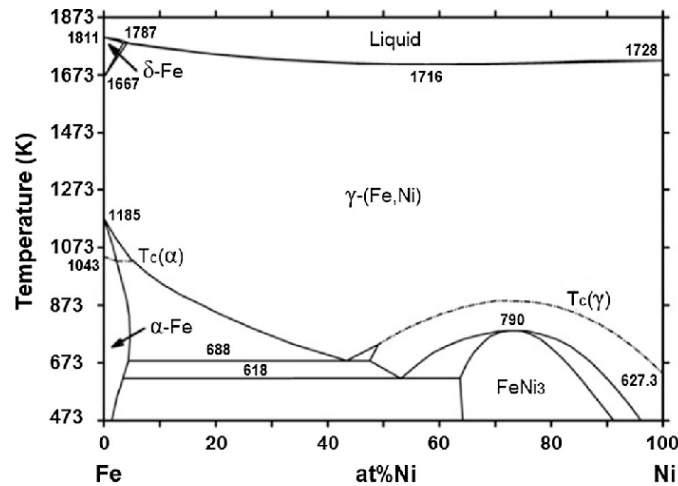


Figure 2. Fe-Ni phase diagram where stable phase equilibria are demonstrated (adapted from [40]).

Table 4. Physical, mechanical, and thermodynamic properties of INVAR-36<sup>®</sup>, according to the literature.

Property	Value					Units
	[51]	[52]	[53] Annealed	[53] CR	[54]	
E	141	146	140	145	141	GPa
$\nu$	0.29	0.28	-	-	0.29	[-]
$\sigma_u$	-	583	448	717	448	MPa
$\sigma_y$	-	-	276	679	276	MPa
HV	-	-	-	-	-	HV
$\epsilon_u$	-	-	35	5.5	-	%
$\rho$	8100	-	-	-	8050	kg/m <sup>3</sup>
$\alpha$	1.8	1.7	-	-	1.3	10 <sup>-6</sup> /K
k	11	11.9	-	-	-	W/m-K

CR—Cold-Rolled,  $\nu$ —Poisson’s coefficient.

Table 5. The chemical composition of INVAR-36<sup>®</sup>, according to the literature.

INVAR-36 <sup>®</sup>	wt%											
	Fe	Ni	C	P	Cr	Mn	Mo	S	Si	Co	Nb	Ti
[51]	Bal.	35–37	≤0.5	0.020	0.500	0.600	0.500	0.025	0.300	-	-	-
[52]	63.4	36.1	0.04	-	0.04	0.16	-	-	0.12	0.06	-	-
[55]	Bal.	35–37	≤0.05	≤0.02	-	0.2–0.6	-	≤0.02	≤0.2	-	-	-
[56]	61.6	35.66	0.22	-	0.01	0.43	-	-	-	-	1.38	0.53

Bal.—balance.

High-quality nanometric finish surfacing is one of the significant challenges when machining INVAR-36<sup>®</sup> since it has low hardness and high chemical activity [44,57]. Hauschwitz et al. [58] suggest that optimizing the rolling torque, polishing speed, and reducing the polishing depth can improve the process’s efficiency and quality while lowering subsurface damage [59,60]. Moreover, some authors have been overcoming these issues thanks to the brisk development of the selective laser melting (SLM) process [61–63] allied to a post-machining process.

### 1.3. HT Steels

HT steels are designed to improve hardness, toughness, and wear resistance through controlled heating and cooling, which is ideal for PIM purposes because they can maintain shape and structural integrity [64,65]. Suitable steels for this purpose, namely AISI H11 (DIN 1.2343), AISI H13 (DIN 1.2344), and AISI L6 (DIN 1.2714) [66], will be addressed in this

paper. AISI H11 (DIN 1.2343) in tooling applications [67] for PIM is especially advantageous as it is a vital material for producing tools and dies. It is classified as air-hardening, high Cr, and premium C-steel and is sturdy and abrasive in wear [68]. AISI H13 (DIN 1.2344) is a highly sought-after hot work tool steel with remarkable strength at high  $T$ . This alloy also has excellent resistance to abrasion at low and high  $T$ , a high level of toughness, a high level of machinability and polishability, and optimal resistance to thermal fatigue [69]. Typically, H13 is utilized in a quenched and tempered state, featuring a microstructure comprising a lath martensitic matrix and secondary-hardening carbide precipitates. This situation brings up challenges when machining, as shown by Figure 3.

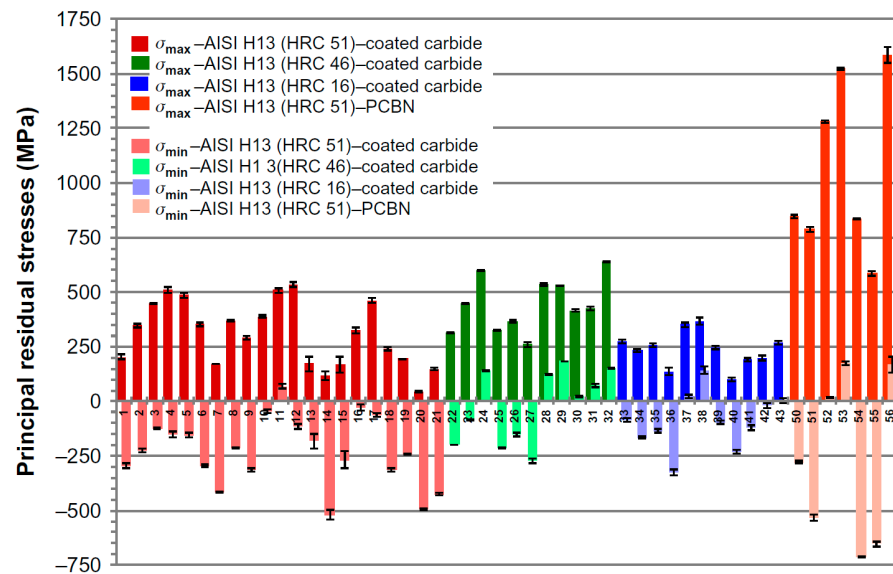


**Figure 3.** Surface residual stresses were investigated during the turning process of H13 (DIN 1.2344) tool steel, employing coated cemented carbide and PcBN cutting tools across 56 distinct cutting conditions [69].

In order to enhance machinability, authors have concluded that the microstructure of H13 produced via AM significantly differs from that of its conventional counterparts. The material’s  $k$  was improved by heat treatment; however, its value depends on the specific parameters of the selective laser melting and post heat treatment process [70,71]. AISI L6 [72] die steel is prominently featured in hot forging manufacturing processes [73], having enhanced properties compared to the H11 and H13 [72] steels. This alloy can also be found in extrusion dies, bolts, casting inserts, forging dies, drop forges, embossing dies, pressure pads, and dies [74]. Table 6 presents the physical, mechanical, and thermodynamical properties of the different HT steels that will be addressed in this work.

**Table 6.** Mechanical properties of HT steels.

Property	Value					Units
	DIN 1.2343 (AISI H11) [75]	DIN 1.2343 (AISI H11) [76]	DIN 1.2344 (AISI H13) [76]	DIN 1.2714 (AISI L6) [77]	DIN 1.2714 (AISI L6) [77]	
E	207	208	210	211	211	GPa
$\nu$					0.27–0.30	[-]
$\sigma_u$	1450–2130	1497	1469	1464	1469	MPa
$\sigma_y$	1200–1850	1303	1265	1255	1253	MPa
HV	448–505				$\geq 649$	HV
$\epsilon_u$	-	16.8	14.2	12.1	18.0	%

Figure 4 illustrates a Typical Time–Temperature–Transformation (TTT) diagram for AISI H11 (DIN 1.2343) steel. Table 7 has some chemical compositions of the AISI H11 (DIN 1.2343), AISI H13 (DIN 1.2344), and AISI L6 (DIN 1.2714) steels, according to the literature, and Table 8 completes the information by presenting each element’s contribution.

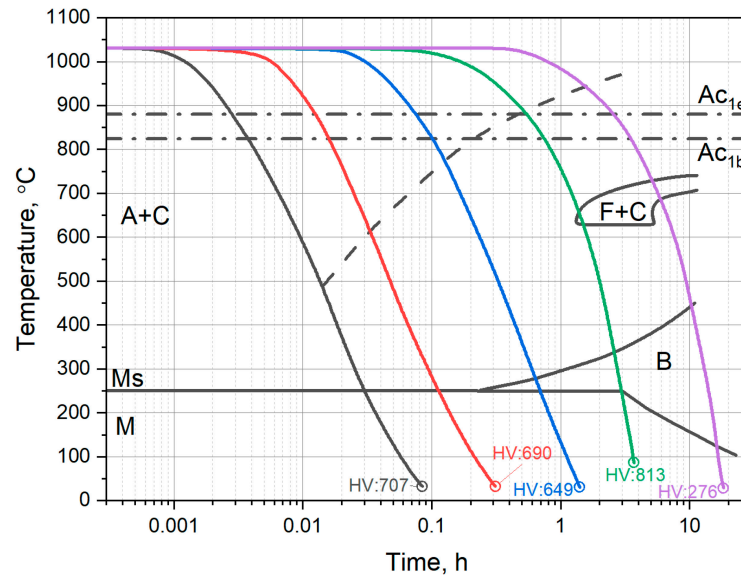


**Figure 4.** Typical Time–Temperature–Transformation (TTT) diagrams (alongside Continuous Cooling Transformation (CCT) diagrams) delineate the onset of phase precipitation in AISI H11 (DIN 1.2343) hot work tool steel. The symbols represent austenite (A), cementite (C), martensite (M), bainite (B), martensite start temperature (MS), ferrite (F), and the initiation (Ac1e) and conclusion (Ac1b) temperatures of austenite transformation [78].

**Table 7.** The typical chemical composition of HT steels, according to the literature.

AISI	H11						H13				L6		
	[75]	[79]	[80]	[81]	[82]	[83]	[84]	[85]	[81]	[77]	[86]	[73]	
Fe	Bal.	Bal.	Bal.	Bal.	Bal.	Bal.	Bal.	Bal.	Bal.	Bal.	94.2–97.0	94.19–97.15	
C	0.37	0.379	0.36	0.38	0.32–0.40	0.39	0.37 ± 0	0.33–0.41	0.38	0.55	0.65–0.75	0.65–0.75	
Cr	5.16	4.64	5.05	5.00	5.13–5.25	5.00	4.95 ± 0.05	4.80–5.50	5.00	0.75	0.6–1.2	0.60–1.20	
Mn	0.27	0.373	0.54	0.40	-	0.32	0.43 ± 0	0.25–0.50	0.40	0.70	0.25–0.8	0.25–0.80	
Mo	1.28	1.23	1.22	1.30	1.33–1.40	1.27	1.22 ± 0	1.10–1.50	1.30	0.50	≤0.50	≤0.50	
Si	≤1.0	1.04	0.97	1.10	1.00	0.88	1.16 ± 0.01	0.8–1.20	1.10	0.25	0.25	0.10–0.15	
V	0.41	0.364	0.38	0.40	1.00	0.93	0.4 ± 0	0.30–0.50	0.90	0.10	0.20–0.31	-	
P	-	0.027	0.015	-	-	0.018	-	-	-	-	-	≤0.03	
S	-	0.005	0.002	-	-	0.007	-	-	-	-	-	≤0.03	
Co	-	0.017	-	-	-	0.01	-	-	-	-	-	-	
Ni	-	0.248	-	-	-	-	0.26 ± 0	-	-	-	1.25–2.00	1.25–2.00	
W	-	-	-	-	-	0.18	-	-	-	-	-	-	

Bal.—balance.

**Table 8.** The characteristics of the main elements of the addressed HT steels [66].

Element	Characteristics
Cu	Increase the $\gamma$ phase domain, Contents higher than 0.3% can cause precipitation hardening, Increases quench penetration, Highly alloyed stainless steels with Cu additions higher than 1% improve resistance to hydrochloric and sulfuric acids.
Be	Energetic deoxidizer, Strongly reduces the $\gamma$ zone, It obtains structural hardening (precipitation hardening), decreasing tenacity.

Table 8. Cont.

Element	Characteristics
Ni	It does not form carbides but is dissolved in the matrix (both in annealed and quenched states), It increases tenacity and resistance to attacks by reducing chemical agents, Decreases $k$ and increases $\rho_R$ .
Co	It does not form carbides, Strongly opposes grain growth at high $T$ , improving tempering stability and heat resistance, Increases $k$ .
C	It improves the hardness and mechanical resistance (annealed) because the reaction of Fe and C forms hard carbides that are resistant to wear, In tempered steels, C is present in the solution in martensite and causes internal stresses responsible for hardness.
Cr	A part is dissolved in the matrix, and the other part is combined with C to form carbides, Chromium carbides increase cutting power and wear resistance, Increases resistance to the action of oxidizing agents.
Mn	Deoxidizer, It does not form carbides dissolved in the matrix, which increases its strength, Increases $\sigma_y$ and $\sigma_u$ .
Mo	Strong carbide former, usually combined with Cr, Mn, Ni, and Co, Reduces brittleness due to tempering in CrNi and Mn steels, Contributes to grain refinement, Increases $\sigma_y$ , $\sigma_u$ , and high- $T$ strength. Decreases resistance to hot oxidation.
Si	Deoxidizer or alloying element, Increases tensile strength and decreases electrical conductivity.

While some chemical elements enhance the final product, others may induce disadvantages. Table 9 summarizes numerous pros and cons of some of the addressed elements from Table 8.

The noteworthy study by Twardowski et al. [87] pertains to the analysis of diverse factors impacting Surface Roughness (SR) after the end milling of hardened steel under High-Speed Milling (HSM) circumstances. It encompasses investigations into milling parameters such as the cutting speed ( $V_c$ ) and axial depth of cut ( $a_p$ , or ADOC), along with exploring process dynamics influencing the SR of machined surfaces. Additionally, an SR model incorporating cutter displacements was developed. The research also examined surface profile charts, focusing on vibrations, and cutting force ( $F_{cut}$ ) components. The investigation revealed that actual SR parameters exhibit values 16 to 25 $\times$  greater than the theoretical values derived from the kinematic–geometric projection of the cutter onto the workpiece. As the theoretical model postulates, the primary determinant of the surface micro-irregularity height and configuration is the feed rate ( $f$ ) rather than the feed-per-tooth ( $f_z$ ). This deviation is ascribed to the milling process dynamics, which are intricately linked to the spindle speed ( $s$ ) frequency. Ensuring the surface quality of injection moulding materials is paramount for achieving optimal performance. Conventional Manufacturing (CM) remains the predominant method for fabricating injection moulds among the three materials addressed. Since they are older and more established machining processes, milling, turning, drilling, and many more are widely employed for shaping and finishing moulds.

Nonetheless, Non-Conventional Machining (NCM), like EDM, can be applied to injection mould manufacturing and enhance the machinability of HPIM. The inquiry originates from its paramount significance within the injection moulding industry, regarding the most common and used materials' machinability. This paper also does not intend to give a broad vision on HPIM to every academic and practitioner but to deliver a structured review able

to contribute to fast knowledge acquisition in the field of HPIM, rendering research in this field invaluable for industry optimization. Following the presentation of the theoretical framework in Section 1, Section 2 delineates the methodology employed in this study, which is based on the Systematic Literature Review (SLR) approach [88] aimed at identifying pertinent papers. In Section 3, these identified papers undergo analysis to present the newer prospects within the research fields of CM and non-traditional machining methods applied to AMPCO<sup>®</sup>, INVAR-36<sup>®</sup>, and HT steels, all injection mould materials. Section 4 discusses findings derived from content analysis, providing an overview of emerging research areas and challenges when machining these types of materials. Section 5 succinctly summarizes the findings and offers a brief outlook.

**Table 9.** Advantages and disadvantages of the main elements of the alloys mentioned above [66].

	Co	Cr	Cu	Mn	Mo	Ni	S	Si
Advantages								
Improve machinability							X	
Improve wear resistance		X		X	X			
Improve tempering resistance	X				X			
Improve <i>T</i> resistance	X	X			X			
Improve hot wear resistance		X			X			
Improve corrosion resistance		X	X		X	X		X
Disadvantages								
Improve corrosion	X		X	X	X	X	X	X
Improve fatigue failure	X	X						
Brittle at high <i>T</i>	X	X						
Low ductility		X		X				
High melting point		X						
High thermal expansion			X					
Improve brittleness	X	X	X	X	X			X
Difficulty in machining					X	X		X

## 2. Materials and Methods

The conceptual map (Figure 5) depicts the methodology for conducting research and gathering information and provides an easily understandable visual representation of all the steps involved in creating this review.

The research and information-compiling phases were carried out through SLR since it is based on a systematic, method-driven, and replicable approach [89,90]. The platform used for SLR was Dimensions.ai, which is connected to all data from Scopus. The method employed for research and data compilation was assessed for quality by considering factors such as citation score and journal impact, and it was systematized. The information sources utilized for this review included ScienceDirect, Springer, MDPI, and ResearchGate platforms, all renowned for their reliability and expertise. To collect data on these subjects, relevant keywords and their combinations were employed, for example, manufacturing processes, machining, conventional, non-conventional, injection moulds, INVAR-36<sup>®</sup>, Fe-Ni36, CuBe, and HT steels. While collecting articles, all critical information was systematized in a table, including processes, names, sources, respective journals, and an indication that it had been used.

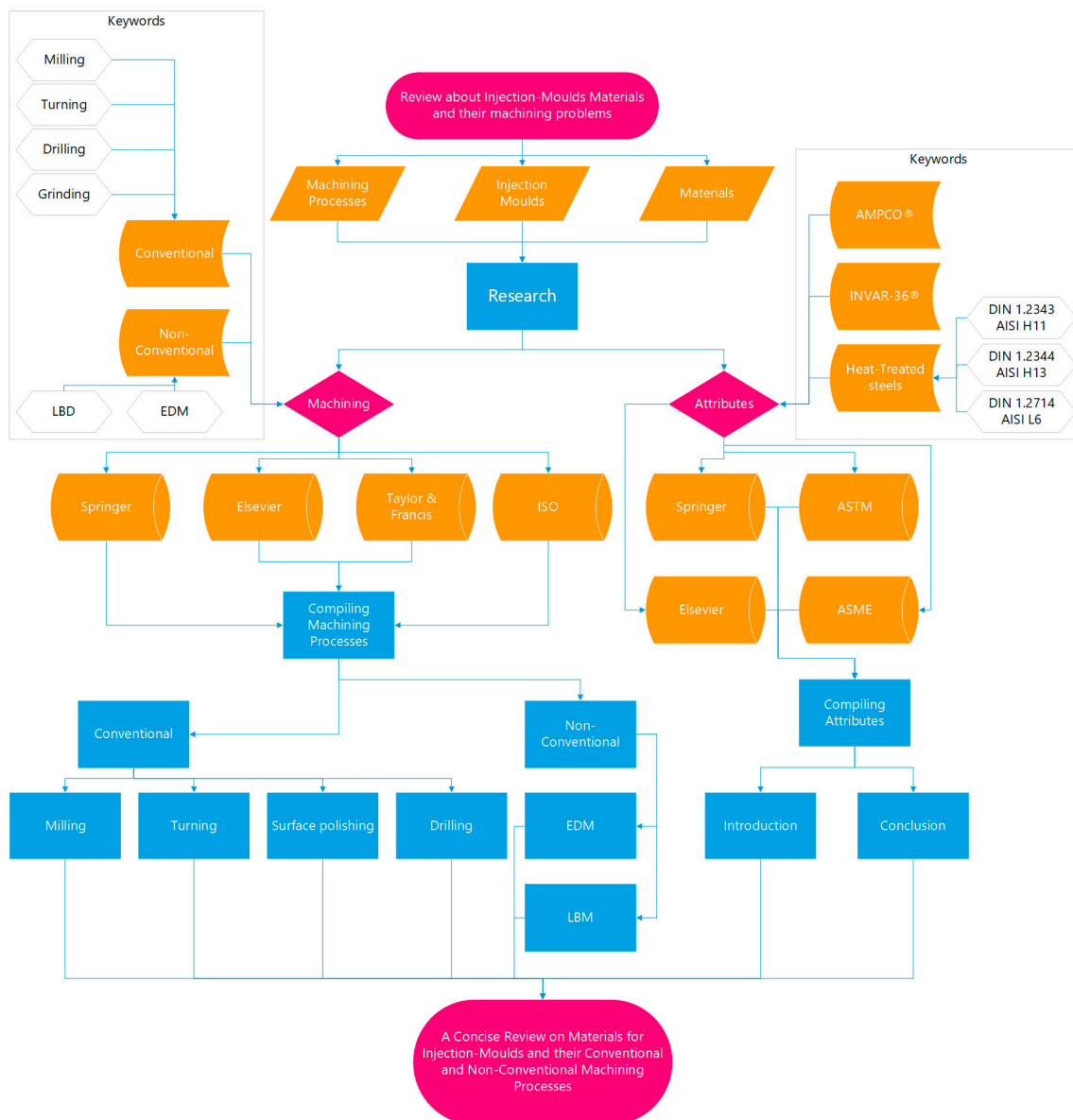


Figure 5. Conceptual map with the methods and research conducted.

### 3. Literature Review

#### 3.1. Conventional Manufacturing (CM)

This section addresses CM processes that allow for the removal of considerable material from the workpiece. The upcoming literature review will focus on the milling, turning, drilling, and boring processes applied to AMPCO<sup>®</sup>, INVAR-36<sup>®</sup>, and HT steels.

##### 3.1.1. Milling

Milling is a crucial manufacturing process that has evolved significantly in recent years [91]. Milling tools come in various forms, including coated and/or uncoated. Coated tools improve the overall process productivity by enhancing the tool life (TL) and production quality of machined components [92]. Nonetheless, for specific applications, uncoated tools have the upper hand, as seen in Lakner et al.'s [93] work, where the cutting performance of uncoated milling tools was superior, producing the highest quality hole surface, the lowest  $F_{cut}$  values, and experiencing the least amount of TW [94,95]. Delamination damage is still a challenge when machining with coated tools. Four techniques were devised by Zou et al. [18] during the helical milling of CFRP/Ti-6Al-4V stacks with coated tools. Based

on experimental data, it was discovered that the extent of delamination damage is linked to the axial cutting load and can be curtailed by altering the sequence of the stacks [96]. It is important to note that a milling process with a high  $f$  can result in surface deterioration caused by the phenomenon known as built-up edge (BUE) [19]. Table 10 addresses some of the most recent state-of-the-art works regarding milling AMPCO<sup>®</sup>, INVAR-36<sup>®</sup>, and HT steels.

**Table 10.** Milling processes: addressed challenges and remarks.

Material	Author	Challenges	Remarks
	Ramesh et al. [32]	The authors assessed the CuBe C17200 [26] alloy in milling operation using a 6 mm carbide end mill. $s$ , $f$ , and $a_p$ were evaluated. The experiments were conducted using an L <sub>9</sub> Taguchi Grey Relational Analysis (TGRA) orthogonal array, and Analysis of Variance (ANOVA) was employed to analyse the influence of the parameters on the arithmetic average of the profile height deviation ( $R_a$ ) and material removal rate (MRR). The Signal-to-Noise (S/N) ratio was employed to find the optimal parameter levels that maximize MRR and minimize $R_a$ .	(1) A higher MRR is achieved at a higher $s$ , $f$ , and lower $a_p$ . A lower $R_a$ is achieved at a medium $s$ , lower $f$ , and higher $a_p$ . A lower MRR will lead to a higher surface finish. (2) The MRR is significantly influenced by $s$ and $f$ . $R_a$ is mainly influenced by $f$ . (3) The optimal parameter levels for maximizing the MRR were $s = 6000$ rpm, $f = 0.85$ mm/rev, and $a_p = 4$ mm. The optimal parameter levels for minimizing $R_a$ were $s = 4000$ rpm, $f = 0.25$ mm/rev, and $a_p = 4$ mm.
AMPCO <sup>®</sup>	Zuo et al. [97]	Several investigations were carried out to examine the impact of $s$ on the TW characteristics of uncoated and TiAlN-coated [98,99] cutting tools. Different $s$ values were tested, and the results revealed that the primary wear mechanism that occurred was adhesive wear, which was responsible for most of the flank wear ( $VB$ ) observed in the tools.	(1) Abrasion decreases the TL and negatively affects the surface finish because of the adhesive TW. (2) The formation of an adhesive layer of material on the tool surface was reported to be directly associated with the wear observed on the tool's flank. (3) The cutting temperature ( $T_{cut}$ ) generated during machining significantly increased adhesive wear on the tool surface, causing notching wear and tool chipping [100].
	Sousa et al. [14]	Evaluated TW after machining a CuBe alloy AMPCOLOY <sup>®</sup> 83, employing solid-carbide uncoated end mills and DLC/CrN multi-layered coated tools, possessing identical geometries. The experimental setups were conducted using an L <sub>9</sub> array with $V_c = 126$ m/min; $f = 350, 750$ , and $1500$ mm/min; $L_{cut} = 18, 36$ , and $48$ m; $a_p = 0.5$ mm, and the radial depth of cut ( $a_e$ or RDOC) was 2.5 mm.	The SR was significantly influenced by $f$ , resulting in a fourfold increase in $R_a$ values when transitioning from $f = 750$ mm/min to $1500$ mm/min. This trend was observed for uncoated and coated tools. The last referred exhibited superior performance for cutting lengths ( $L_{cut}$ ) up to 36 m. Conversely, uncoated tools consistently provided better surface quality for $L_{cut} = 48$ m. The wear behaviour of the tools was similar, $VB = 80.71$ $\mu$ m and $VB = 102.3$ $\mu$ m for uncoated and coated tools at $L_{cut} = 48$ m, respectively, exhibiting increased and pronounced $VB$ at $f = 1500$ mm/min. At $L_{cut} = 18$ and $36$ m, the coated tools revealed less $VB$ than uncoated ones. Regarding TW mechanisms, adhesion, tool chipping, and abrasion were identified as the principal wear mechanisms. Additionally, coating delamination was observed in the coated tools. Tool chipping and cutting-edge breakage were more prevalent at higher $f$ values, affecting coated and uncoated tools.

Table 10. Cont.

Material	Author	Challenges	Remarks
AMPCO®	Nogueira et al. [34]	Conducted an assessment, identification, and quantification of TW mechanisms during the machining of AMPCO® using WC-Co uncoated tools and TiAlTaN-coated tools by Physical Vapour Deposition (PVD) [101,102]. The experimental setups were conducted using an L <sub>6</sub> array with $V_c = 126$ m/min; $f = 750$ and $1500$ mm/min; $L_{cut} = 26.8, 53.6,$ and $73.7$ m; $a_p = 0.5$ mm and $a_e = 3.6$ mm. The primary objectives were to evaluate tool performance under varying $L_{cut}$ and $f$ at three distinct levels and to analyse SR on the machined surface.	For WC-Co uncoated tools, $f$ and $L_{cut}$ parameters noticeably influence the $R_a$ values. The lowest $R_a$ values were observed under $f = 750$ mm/min and $L_{cut} = 26.8$ m, while the highest $R_a$ values were noted for $f = 1500$ mm/min and $L_{cut} = 73.7$ m, both longitudinally and transversely. This suggests that the superior $R_a$ , the total height of the profile ( $R_t$ ), and the maximum height of the profile ( $R_z$ ) values were achieved at lower $f$ and $L_{cut}$ values, indicating that a poorer machined surface quality was obtained for higher $f$ and $L_{cut}$ values. Concerning $VB$ , the primary wear mechanisms identified were the abrasion and adhesion of the machined material. For TiAlTaN-coated tools, the $R_a$ values and trends were consistently higher than those of the WC-Co uncoated tools. Regarding $VB$ , the primary wear mechanisms identified were delamination, chipping, and abrasion.
	Zheng et al. [103]	A trialled face milling experiment was conducted on INVAR-36® using a coated carbide. The microhardness was assessed, and the metallographic structure was observed to identify work-hardening mechanisms.	Work-hardening occurred during the face milling of INVAR-36®, ranging from 120 to 150% at a 30 µm depth. Parameters such as $a_p$ and $f_z$ significantly influenced the degree and depth of work-hardening. As these parameters increased, the depth and degree of work-hardening also increased. Upon metallographic observation, the work-hardening layer comprised two distinct regions: the thermal-force-influenced and force-influenced.
INVAR-36®	Cornelius et al. [104]	These authors elucidated the definition and transfer of the coordinate system for the five-axis machining of additively manufactured preforms. The practical application of this method was demonstrated through the precision machining of a mould for a Carbon Fibre-Reinforced Polymer (CFRP) layup fabricated from an additively manufactured INVAR-36® preform.	The utilization of this technique holds the potential to enhance accuracy, minimize material wastage, and reduce the overall machining cycle time. However, the final machined component proved unsuitable when applied to the Wire Arc Additive Manufactured (WAAMed) INVAR-36® preform examined in this study. This outcome was attributed to several inherent challenges associated with additively manufactured parts, including warping, internal stresses, and porosities.
	Gil Del Val et al. [105]	A study characterizing the machinability of INVAR-36® samples produced through Wire Arc Additive Manufacturing (WAAM) technology was proposed, employing Minimum Quantity Lubrication (MQL) during the finishing milling process.	The SR values of WAAM samples are minimal under all cutting conditions, despite a 9% increase in average $F_{cut}$ compared to wrought samples, attributed to the higher hardness level of WAAM samples (20%). Furthermore, the statistical analysis not only underscores the negligible influence of $V_c$ on machinability but also identifies the optimal roughness value (0.8 µm) achieved at $V_c = 50$ m/min and $f_z = 0.06$ mm/tooth. Ultimately, the predominant wear mechanism observed during the finishing milling of WAAM INVAR-36® samples is adhesion on the rake and clearance faces (RF and CF).

Table 10. Cont.

Material	Author	Challenges	Remarks
HT Steels	Arruda et al. [3]	This work aimed to optimize $R_a$ on AISI H13 (DIN 1.2344) steel, using a ball nose end mill, during finishing milling. $R_a$ was evaluated in two cutting directions.	The ball nose end mills can effectively produce suitable $R_a$ values for manufacturing moulds and dies when used for the finishing milling of AISI H13 hardened steel. The outcomes of this investigation can be applied in the finishing milling process of AISI H13 hardened steel using ball nose end mills to obtain consistent $R_a$ values that are robust against noise factors.
	Singh et al. [106]	The impact of machining parameters during the milling of AISI H11 (DIN 1.2343) was assessed by evaluating SR and MRR. TGRA with a standard $L_{27}$ orthogonal array was conducted to determine the optimal milling setup. Data analysis was conducted using Microsoft® Excel™ software, and the significance of the model was assessed using the ANOVA method.	(1) $V_c$ emerges as the sole significant machining parameter affecting SR. Increasing $V_c$ leads to enhanced SR. (2) $V_c, f$ , and $a_p$ significantly influence the MRR, which rises with increasing values of the input parameters. These parameters are significant factors impacting the composite response, comprising SR (with a weightage of 0.2) and the MRR (with a weightage of 0.8), albeit with unequal weighting. (3) In rough machining conditions, $f$ is the most influencing, followed by $a_p$ and $V_c$ . (4) $V_c$ and $f$ emerge as significant parameters in finishing conditions, while $a_p$ is deemed insignificant.
	Şahinoğlu [107]	This author investigated the vibration, energy consumption, power consumption ( $P_{in}$ ), and SR values during the machining of AISI H11 (DIN 1.2343) tool steel under cryogenic $CO_2$ ( $l$ ), coolant, and dry cutting lubricating environments.	Vibration values increase with extreme cutting parameters, with the highest vibration occurring during $CO_2$ ( $l$ ) cutting. The coolant environment exhibits the slightest vibration. $f$ is determined to be the most influential parameter on SR. The optimal cutting conditions for reduced vibration and SR values were identified as $a_p = 0.2$ mm, $V_c = 175$ m/min, and $f = 0.119$ mm/rev with coolant lubrication. Under these conditions, vibration, SR, and $P_{in}$ were reduced by 5.18%, 37.12%, and 36.19%, respectively, and machine efficiency increased by 7.16%. It is noteworthy that other authors have also studied the subject of machining vibrations [108,109] regarding other materials.
	Platt et al. [110]	These authors conducted a study on the High-Feed Milling (HFM) of surface structures in components made of AISI H11 (DIN 1.2343) hot work tool steel (HWS). The process's performance was assessed through $F_{cut}$ measurements and TL tests. The resulting surface topography was measured and assessed based on the quality of the structure and roughness parameters.	$V_c = 200$ m/min resulted in reduced $F_{cut}$ and TW development compared to $V_c = 100$ m/min. Higher values for the lead angle ( $\beta_f$ ) also contribute to decreased $F_{cut}$ while altering the resulting structure geometry. Increasing $a_p$ reinforces these trends. Significant differences are observed in the achievable $R_z$ and their qualitative geometry, along with anisotropies in the structure formation, concerning the surface topography. Additional investigations are required to assess burr formation associated with VB in HFM.

Table 10. Cont.

Material	Author	Challenges	Remarks
HT Steels	Wojciechowski et al. [111]	During the precise ball-end milling of AISI L6 (DIN 1.2714) alloy steel, the ploughing phenomenon was assessed by analysing $F_{cut}$ at the interface between the tool flank face and the workpiece. A novel ploughing $F_{cut}$ model was developed for ball-end milling, accounting for the influence of the minimum uncut chip thickness ( $h_{min}$ ) and the ploughing volume.	The ploughing $F_{cut}$ was significantly higher when milling with a worn tool, due to the irregular non-circular profile of the cutting edge below the stagnant point and the presence of attrition and micro-grooves on the tool flank face. The angle that represents the slope of the machined surface was found to have a non-linear impact on the estimated values of $h_{min}$ and $k$ . When using a worn tool, $VB = 150 \mu\text{m}$ [112], it was observed that the $h_{min}$ value increased, directly linked to the significant growth of the cutting-edge radius.
	Abu Bakar et al. [113]	These authors conducted an experimental study to investigate TW mechanisms during the dry and cryogenic $N_2(l)$ milling of AISI H13 (DIN 1.2344) steel, employing different cutting-edge radii. The objective was to examine how the cutting-edge radius influences the TW mechanism of uncoated carbide-cutting tools with rounded edges.	The milling setup is determined by $V_c = 200 \text{ m/min}$ , $f_z = 0.03 \text{ mm/tooth}$ , and $a_p = 0.1 \text{ mm}$ for dry and cryogenic $N_2(l)$ cooling environments. Milling using $N_2(l)$ with a tool that has a cutting-edge radius of $R_n = 0.03 \text{ mm}$ enhances the performance of an uncoated carbide tool during the milling of AISI H13 (DIN 1.2344) steel. This reduces TW rates and extends TL compared to dry machining with a commercial tool of $R_n = 0.018 \text{ mm}$ . $N_2(l)$ dissipating heat efficiency delays the development of TW. A larger cutting-edge radius significantly impacts the TL, attributed to the higher $VB$ generated at a sharper cutting edge. Analysis using Field-Emission Scanning Electron Microscopy (FESEM) revealed that abrasive and adhesive wear were the predominant wear mechanisms observed under dry and cryogenic $N_2(l)$ milling, being more pronounced in dry machining due to high $T$ .

Figures 6 and 7 from Nogueira et al.'s [34] and Sousa et al.'s [14] works, respectively, depict the associated wear mechanisms in the tools used when milling AMPCO®.

### 3.1.2. Turning

Turning is a machining technique that has become increasingly popular in industrial manufacturing. The process presents challenges, such as the TW and tear of the coated inserts over time, affecting the surface and subsurface properties of the workpiece [114,115]. The tool–workpiece interaction is a critical aspect to consider in hard turning [116,117]. While hard turning offers benefits in terms of productivity, it is essential to consider the resulting properties of the workpiece: SR, dimensional and geometric tolerances, residual stress, surface and bulk hardness, and the microstructure of the surface layers. According to Meyer et al. [118], the effective contact dimensions at the primary cutting edge are essential to characterize the complex turning process. Adjustments in finishing, nominal process parameters,  $a_p$ , and  $f$  are imperative to obtain the best results [118–120].

Although orthogonal cutting is not the most used process when manufacturing injection moulds, it is intended to provide in Table 11 some of the most recent state-of-the-art works regarding the challenges other researchers felt, which can be extrapolated to milling situations.

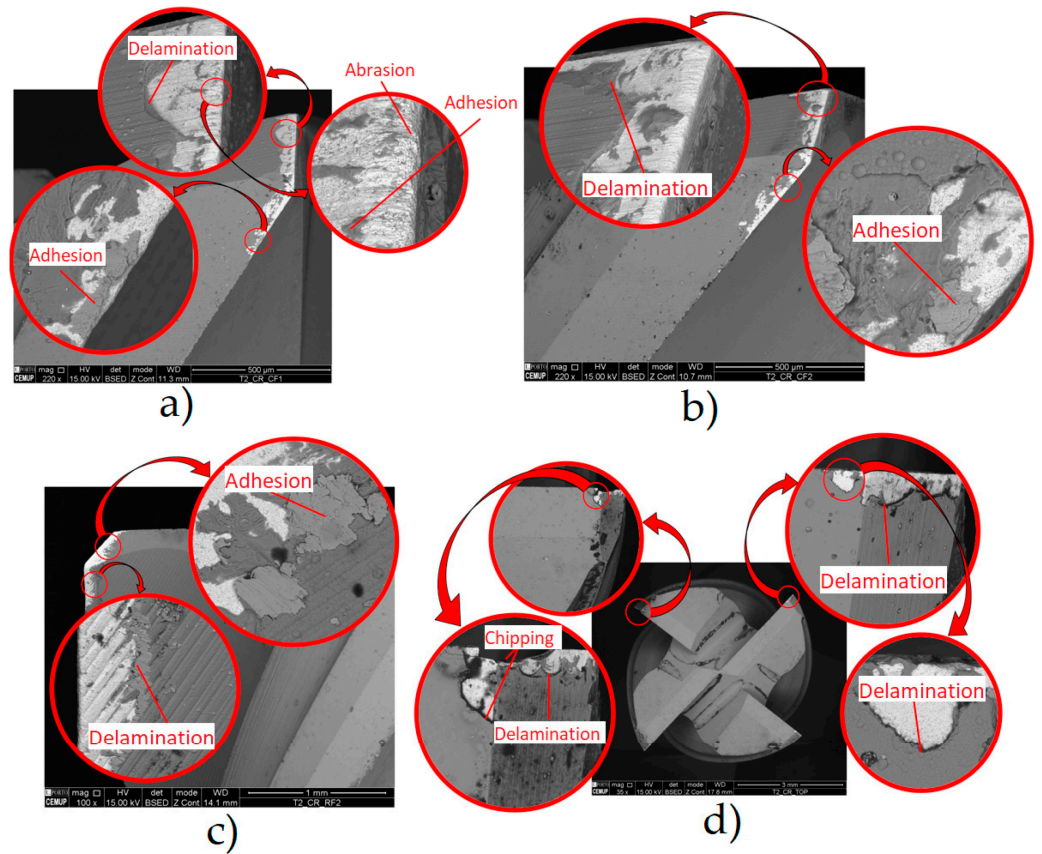


**Figure 6.** SEM images of a TiAlTaN-coated tool during testing at  $L_{cut} = 53.6$  m and  $f = 750$  mm/min. Magnifications of 100× and 220× of the following: (a) Tooth 1 of the cutting tool with CF, (b) Tooth 2 of the cutting tool with CF, (c) Tooth 2 of the cutting tool with RF, and (d) the top surface [34].

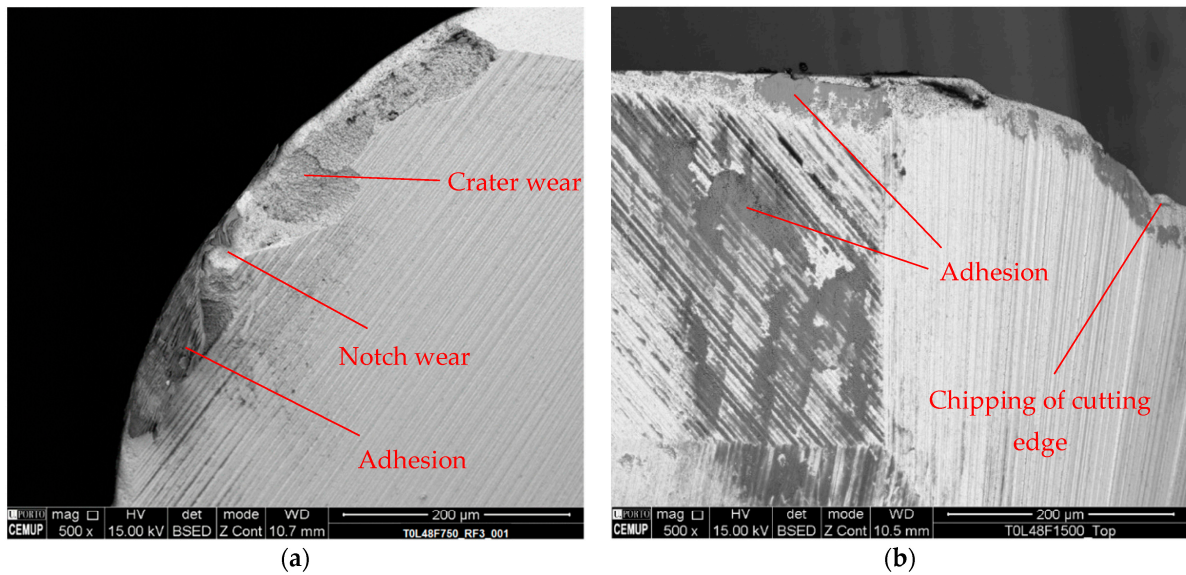


**Figure 7.** (a) Wear mechanisms observed on the RF of an uncoated tool during testing at  $L_{cut} = 48$  m and  $f = 750$  mm/min. (b) Wear mechanisms detected on the top surface (TOP) of tools employed by an uncoated tool during testing at  $L_{cut} = 48$  m and  $f = 1500$  mm/min [14].

Table 11. Turning processes: addressed challenges and remarks.

Material	Author	Challenges	Remarks
AMPCO®	Sharma et al. [121]	These authors employed a molecular dynamics simulation to investigate the interaction between the tool and hard particles during the nano-orthogonal cutting of CuBe. They observed that including hard particles within the workpiece materials influences the cutting process, impacting surface formation, material deformation, and TW mechanisms.	The position and dimensions of a hard particle are determining factors in surface formation and subsurface damage. $F_{cut}$ experienced sudden increases, leading to surface deterioration. Subsequently, the particle rebounds after the tool passage, causing protrusions on the surface. Shockley partial dislocations emerge as the primary plastic deformation mode during CuBe cutting. If the particle size exceeds the sharpness of the cutting edge, dislocations glide into the bulk material, resulting in subsurface damage. The interaction between hard particles and the diamond tool during cutting amplifies equivalent stresses, resulting in the removal of carbon atoms from the tool. The density of dislocations is highest for the (111, $\langle 110 \rangle$ ) orientation and lowest for the (100, $\langle 100 \rangle$ ) orientation. A more significant degradation of the tool edge is observed in the last referred orientation.
	Sharma et al. [31]	These authors examined the mechanisms involved in machining Cu and CuBe alloys by analysing imprints on the tools and machined surfaces. In addition, the authors investigated factors such as TL, wear patterns, changes in the diamond tool's phase, and the interactions between the tool and workpiece materials during the machining process.	(1) CuBe has a high $VB$ rate, which means that the roughness increase is also high as a reflection of the rate affecting the surface. (2) Because of the high $VB$ rate, the increase in $R_a$ is approximately 300% compared to the initial values. (3) Comparing Cu with CuBe, the latter has a much higher wear rate. (4) The TL and $R_a$ of CuBe are 52% higher than Cu. (5) The primary mechanism responsible for wear at the edge of diamond tools is stress-induced amorphization, which transforms the diamond material from a crystalline to amorphous state.
INVAR-36®	Zhao et al. [122]	These authors focused on the cutting performance of ceramic cutting tools in wet turning the INVAR-36® alloy, including TL, $R_a$ , and failure mechanisms. The optimal cutting parameters were determined using an orthogonal test and range analysis.	Parameter $a_p$ significantly impacted the metal MRR amount, while $f$ significantly affected $R_a$ . The observed wear mechanisms included abrasive, diffusion, and oxidation wear. The log-normal distribution was suitable to characterize the TL distribution, with a coefficient of variation of 0.085, suggesting the TiB <sub>2</sub> -SiC ceramic cutting tools have high reliability when continuously wet turning the INVAR-36® alloy using the optimized cutting parameters.
	Mahir [123]	The performance of three distinct tools was compared: a two-layered TiCN-Al <sub>2</sub> O <sub>3</sub> -coated tool, a single-layered TiAlN-coated tool, and one uncoated tool when machining INVAR-36®. The TW is about 30% and 60% better using the TiCN-Al <sub>2</sub> O <sub>3</sub> -coated insert than the single-layer TiAlN-coated and uncoated inserts, respectively.	(1) $VB$ and BUE were the predominant wear mechanisms observed for all cutting tools. (2) In the machining of the INVAR-36® alloy, all tools showed a significant decrease in cutting time as $V_c$ increased. (3) The developed first- and second-order models successfully estimated the output parameters ( $F_c$ , $R_a$ , $VB$ , and $P_c$ ) with a high Pearson's correlation coefficient ( $R^2$ ), (4) The outcomes of this study show that the two-layer TiCN-Al <sub>2</sub> O <sub>3</sub> -coated insert significantly improves the cutting performance of the INVAR-36® alloy compared with uncoated and single-layer TiAlN-coated inserts. Multi-layer cutting tools should be used to avoid a premature loss of cutting tool performance, and cutting parameters should be selected at moderate levels.

Table 11. Cont.

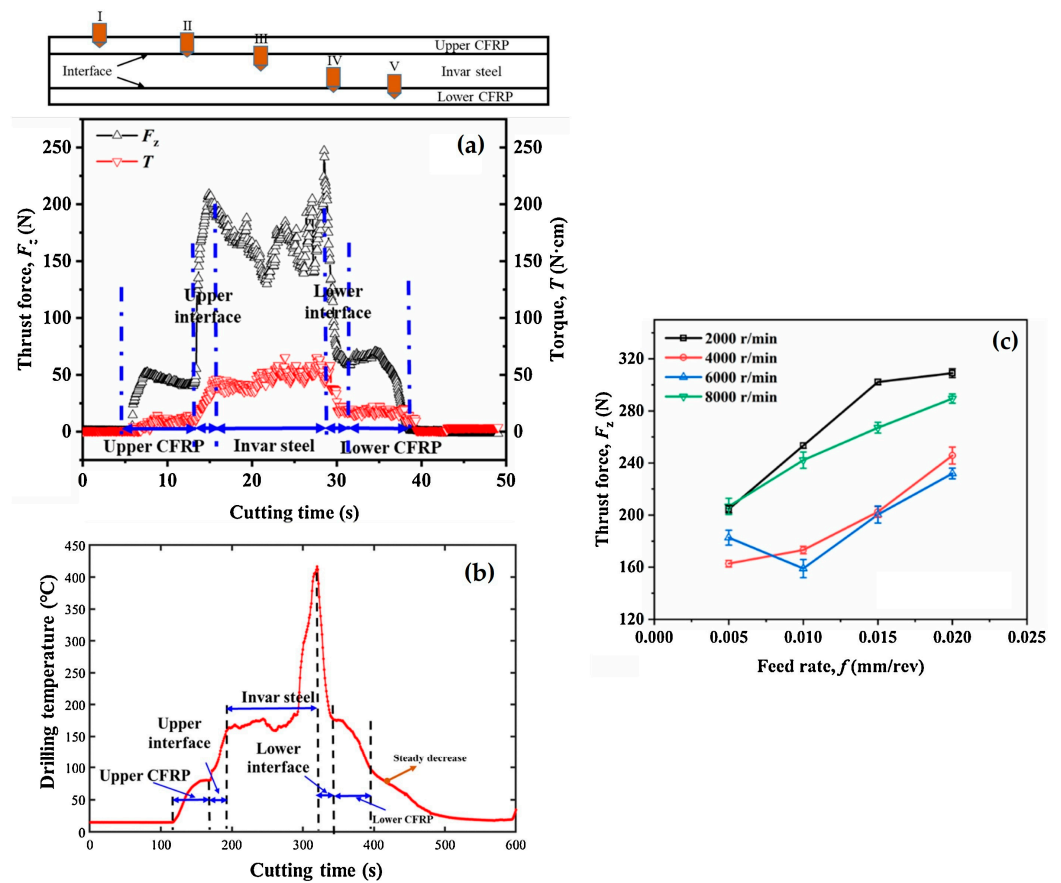
Material	Author	Challenges	Remarks
	Suresh and Basavarajappa [124]	This work is focused on formulating a response surface methodology to represent the relationship between cutting parameters and the turning process of hardened AISI H13 (DIN 1.2344) steel (55 HRC) using TiCN-coated ceramic tools under dry cutting conditions. Mathematical models were developed to correlate machining parameters with TW and SR.	The central composite design utilized in this study has demonstrated its effectiveness in modelling TW and SR. $V_c$ is the most significant parameter affecting TW, accounting for 47.4% of the variance, followed by $f$ at 28.15% and $a_p$ at 15.8%. Abrasion is identified as the primary wear mechanism observed under extreme cutting conditions, while adhesion predominates at softer cutting conditions. Regarding SR, $f$ emerges as the most influential factor, explaining 49.55% of the variance, followed by $V_c$ at 40.3% and $a_p$ at 8.8%. SR improves with increasing $V_c$ but deteriorates with higher $f$ .
HT Steels	Benlahmidi et al. [125]	The impacts of $V_c$ , $f$ , $a_p$ , and workpiece hardness on SR, cutting pressure, and cutting power were investigated during hard turning hardened AISI H11 (DIN 1.2343) utilizing cBN7020 tools.	Factors and performance relationship measures are expressed through quadratic regression equations, enabling the estimation of the expected performance. The mathematical models demonstrate a good fit with experimental values within a 95% confidence interval. The hardness of the machined material predominantly influences the variations in output factors. This insight has facilitated the precise delineation of the hard turning domain for the proposed cBN tool and workpiece. The presented results indicate a significant improvement in SR with increasing $V_c$ and workpiece hardness while displaying adverse effects with a higher $f$ , although $a_p$ has a negligible influence. The optimal setup is $V_c = 178.32$ m/min, $f = 0.08$ mm/rev, $a_p = 0.43$ mm, and a workpiece hardness of 41.73 HRC. Additionally, it was determined that TL is primarily influenced by $V_c$ , with a 91.68% contribution and to a lesser extent by $f$ , with a 3.83% contribution.
	Liu et al. [126]	TiCN-based cermets and cemented carbide tools were manufactured with a multi-layer TiN/ $Al_2O_3$ /TiCN/TiN CVD coating to evaluate their performance in the orthogonal cutting machining of hardened AISI H13 (DIN 1.2344) steel.	(1) An increase in $V_c$ , $a_p$ , and $f$ accelerates VB. Coated cermets exhibit a longer TL than uncoated ones. However, with increasing $a_p$ and $f$ , $F_{cut}$ significantly rises. Due to poor toughness, cracks are more prone to initiate and propagate in coated cermets, resulting in a shorter TL. (2) At $a_p = 0.2$ mm and $f = 0.05$ mm/rev, coated cermets demonstrate the most extended lifespan when the spindle rotations ( $n$ ) exceed 700 rpm. The exceptional diffusion and adhesion TW resistance of coated cermets at high $T$ contribute to the improved SR of the workpiece.

Table 11. Cont.

Material	Author	Challenges	Remarks
HT Steels	Özbek [127]	This author explored how cryogenic treatment affects the performance of cutting tools when turning AISI H11 (DIN 1.2343) steel. This treatment resulted in an increased hardness of the cutting tools.	The cutting tools that underwent deep cryogenic treatment experienced the most substantial increase in hardness, with a rise of 10.87%. The wear resistance of tungsten carbide cutting tools coated with TiCN-Al <sub>2</sub> O <sub>3</sub> -TiN was enhanced through cryogenic treatment. Tools subjected to deep cryogenic treatment demonstrated a superior wear resistance and $R_a$ compared to those treated with shallow cryogenic treatment for six hours. As $V_c$ increased, the cutting tools exhibited an increased $VB$ . The abrasive TW mechanism resulted in $VB$ on all tools, while the adhesive wear mechanism caused a built-up edge on the tools. Cryogenically treated tools induced superior $R_a$ values on the workpieces compared to untreated tools. Tools that underwent deep cryogenic treatment for 24 h achieved the most optimal $R_a$ . The experimental findings indicated that cryogenic treatment enhanced the cutting tool's resistance to abrasion.

### 3.1.3. Drilling

Drilling is crucial in manufacturing and assembling parts used in various industries, including PIM [128]. Reduced hole quality and degraded drills due to the significant  $F_{cut}$  and  $T_{cut}$  during the process are still great challenges due to the tear of drill bits. According to Ortner and Kromoser [129], the effect of the drill diameter on  $F_{cut}$  is not significant at a low  $V_c$ , but for a higher  $f$ , an apparent increase in the influence can be observed [129,130]. Newer technologies like Ultrasonic Vibration Drilling (UVD) offer high efficiency, good stratum adaptability, and a fast drilling speed. Ma et al. [131] investigated four different types of drilling in a Ti6Al4V alloy: Direct Drilling (DD), Peck Drilling (PD), UVD, and Ultrasonic Vibration Peck Drilling (UVPD). UVD could still obtain a smaller axial force ( $F_a$ ) than DD, and  $F_a$  continued to decline with the increased vibration amplitude. When the amplitude was increased from 0 to 5.5  $\mu\text{m}$ , the mean thrust force decreased by 41.8 N, about 18.6%. The major drawback is that mathematical models and Finite Element Analysis (FEA) are needed to study the longitudinal vibration characteristics of the drill when machining in overburden layers. Based on the mechanical vibration theory, a model considering the stratum coupling boundary and vibration head is paramount to be established, according to Li et al. [132]. Table 12 addresses two state-of-the-art works regarding drilling INVAR-36<sup>®</sup> and HT steels. It is noteworthy that there is a gap in the literature around HT steels' drilling and the most about AMPCO<sup>®</sup> is conducted by Electro-Discharge Drilling (EDD).



**Figure 8.** The progression of the (a) thrust force and (b)  $T_{cut}$  signals as the tool advances during single-pass drilling; (c) the evolution of thrust forces with various processing parameters in the INVAR-36<sup>®</sup> layer [133].

**Table 12.** Drilling processes: addressed challenges and remarks.

Material	Author	Challenges	Remarks
INVAR-36 <sup>®</sup>	Zhang et al. [133]	<p>These authors endeavoured to elucidate the progression of crucial cutting phenomena, such as thrust forces, <math>T_{cut}</math>, and surface quality while drilling holes in INVAR-36<sup>®</sup>/CFRP T700 multi-material stacks, focusing on the influence of cutting parameters. Additionally, the mechanism governing the control of the interfacial drilling response was examined. PVD TiAlN-coated drills were used, and the machining levels were defined by <math>s = 2000, 4000, 6000,</math> and <math>8000</math> rpm/min, and <math>f = 0.005</math> mm/rev, <math>0.01</math> mm/rev, <math>0.015</math> mm/rev, and <math>0.02</math> mm/rev. Only the findings about INVAR-36<sup>®</sup> will be addressed.</p>	<p>(1) The thrust forces and <math>T_{cut}</math> encountered during the drilling of the INVAR-36<sup>®</sup> phase surpass those observed in both the upper and lower CFRP phases (Figure 8a,c).</p> <p>(2) The INVAR-36<sup>®</sup> alloy's <math>k</math> deviates from that of conventional engineering materials, resembling that of non-metallic materials like ceramics. Consequently, drilling INVAR-36<sup>®</sup> generates more heat during cutting, resulting in a comparatively higher <math>T_{cut}</math>. A significant amount of cutting heat is transferred to the chip, rendering the INVAR-36<sup>®</sup> alloy chip soft and susceptible to adhesive TW (Figure 8b)</p> <p>(3) As the drill advances, the chip from the INVAR-36<sup>®</sup> alloy accumulates and adheres to the drill bit, exacerbating the rubbing of the drill against the material.</p> <p>(4) Ensuring the processing quality of the INVAR-36<sup>®</sup> alloy poses challenges due to its high plasticity, toughness, and low <math>k</math>.</p>

Table 12. Cont.

Material	Author	Challenges	Remarks
HT Steels	Sorgato et al. [134]	The TW and surface quality in drilling operations of multi-layered cladding were investigated, which is particularly challenging and requires further investigation. The laser cladding of AISI H13 (DIN 1.2344) tool steel layers using varying powder sizes and laser power was performed. Later, drilling tests at constant cutting parameters were conducted to evaluate drill bit wear. Additionally, the study investigated the quality of the drilled holes by analysing the internal $R_a$ and edge contour and their relationship with TW.	The accuracy of the drilled holes' diameter and their internal surface finish quality were evaluated. The primary wear mechanisms identified were adhesion, the coating peeling off, and laser cladding samples at the slowest scanning speed experienced BUE on the tool's cutting edges. The improved mechanical properties obtained at lower scanning speeds generate more heat in the cutting zone, increasing BUE formation. The results indicate that the microstructural features induced by the deposition process significantly impacted the TW and the quality of the drilled hole when using laser cladding AISI H13 tool steel. The parameters used for laser cladding significantly impact TW and, consequently, the quality of the drilled hole.

### 3.1.4. Surface Polishing

Traditional methods like lapping, polishing, and honing are prevalent in the industry, yet they present limitations such as subsurface damage, residual stress, and challenges in finishing complex and free-form surfaces. However, various advanced finishing techniques have been explored in pursuit of attaining damage-free, nano-level, or angstrom-level surface finishes on challenging materials. These include Abrasive Flow Finishing (AFF), Chemical Mechanical Polishing (CMP), Elastic Emission Machining (EEM), Magnetic Abrasive Finishing (MAF), Magnetorheological Finishing (MRF), and Plasma-Assisted Polishing (PAP) [135]. Electrolytic polishing is exclusively viable for metals. It is influenced by the preceding mechanical background of the surface, shedding light on the mechanisms involved in the mechanical abrasion processes [136]. Table 13 addresses some of the most recent state-of-the-art works regarding surface polishing AMPCO<sup>®</sup>, INVAR-36<sup>®</sup>, and HT steels.

Table 13. Surface polishing processes: addressed challenges and remarks.

Material	Author	Challenges	Remarks
AMPCO <sup>®</sup>	Kityk et al. [137]	Research on electropolishing bronze using an electrolyte composed of a deep eutectic solvent known as Ethaline was conducted. This solvent comprises a eutectic blend of choline chloride and ethylene glycol in a 1:2 mass ratio. Two types of bronze alloys, namely AMPCO <sup>®</sup> 22 and AMPCO <sup>®</sup> 712, were employed in the study.	Electropolishing AMPCO <sup>®</sup> 22 and AMPCO <sup>®</sup> 712 can be carried out in Ethaline at an electrode potential of +2.5 V and $T = 25\text{ }^{\circ}\text{C}$ for 20 min. The SR was reduced by 80% and 60% compared to its initial values for AMPCO <sup>®</sup> 22 and AMPCO <sup>®</sup> 712, respectively. Additionally, the electropolished surfaces of AMPCO <sup>®</sup> 22 and AMPCO <sup>®</sup> 712 showed improved corrosion resistance by nearly 30% and 10% for AMPCO <sup>®</sup> 22 bronze and AMPCO <sup>®</sup> 712 bronze, respectively.

Table 13. Cont.

Material	Author	Challenges	Remarks
INVAR-36®	Wang et al. [138]	A numerical investigation was performed to ascertain the primary factors influencing the nano-polishing characteristics of INVAR-36®. Given its low hardness and pronounced chemical reactivity, achieving superior surface quality with nanometric precision presents a formidable challenge. FEA was employed via a molecular dynamics simulation, complemented by an experimental validation of the simulation outcomes.	<p>(1) Within the molecular dynamics simulations, elevating the polishing velocity yielded an increased MRR and mitigated subsurface damage. However, this also led to a coarser groove surface and encouraged the formation of amorphous regions. As the speed escalated further, the polishing efficiency reached a critical threshold.</p> <p>(2) During polishing with rolling abrasives, augmenting the rolling torque correlated with a heightened workpiece <math>T</math> and diminished the polishing force and MRR.</p> <p>(3) Rolling motion engenders a higher <math>T</math>, reduced MRR, and a rougher surface morphology relative to the sliding motion. At greater polishing depths, ploughing and cutting removal are the principal removal mechanisms in pure sliding processes. Conversely, ploughing manifests only at deeper polishing depths in a rolling motion, and the ploughing regime signals are less pronounced than those in a pure sliding motion.</p>
	Temmler et al. [139]	The impact of multi-step laser polishing on the microstructural characteristics of the remelted surface layer of AISI H11 (DIN 1.2343) tool steel was examined. Four distinct sets of process parameters were chosen for the laser polishing initially annealed samples composed of H11 tool steel.	Electron Backscatter Diffraction (EBSD) analysis demonstrated a refinement in grain structure, with an average size ranging from 1.1 to 1.5 $\mu\text{m}$ after remelting using the laser. Surface hardness significantly increased the hardness of the initially soft annealed base material, attributed to grain refinement and the formation of martensite. SR measurements revealed $R_a = 0.11 \mu\text{m}$ achieved within an Ar atmosphere. Introducing 6 vol% $\text{CO}_2$ into the process gas atmosphere further reduced $R_a = 0.05 \mu\text{m}$ .
HT Steels	Awale et al. [140]	The capability of non-destructive methods such as micromagnetic Barkhausen Noise (MBN) in evaluating grinding burn defects concerning the microstructural and mechanical characteristics of hardened AISI H13 (DIN 1.2344) die steel was discussed. The study employed an MQL lubrication grinding environment, utilizing environmentally friendly machining fluids such as Paraffin Oil (PO) and castor oil (CO) and compared their efficacy with traditional wet and dry grinding methods.	A 75% decrease in grinding $T$ accompanied by minimal oxidation and carbonization layers, $C = 3.16\%$ and $O = 1.23\%$ , occurred at higher $f = 12 \text{ m/min}$ . This was facilitated by adequate lubrication and cooling during the wheel-work-chip interaction through the capillary penetration of castor oil-based MQL, as observed in dry grinding. The MQL-CO grinding method exhibited the lowest $R_a = 0.232 \mu\text{m}$ and $R_z = 1.838 \mu\text{m}$ on the surface topography. This was attributed to the superior anti-friction and anti-wear properties of CO, which mitigated ploughing and rubbing actions. Dry grinding resulted in notable alterations in the microstructure, with a thermal damage region of 55 $\mu\text{m}$ and a lower microhardness, 429 HV, due to temper damage effects on the ground surface and subsurface at elevated $T = 817 \text{ }^\circ\text{C}$ . A non-destructive assessment revealed a poor MBN signal and small envelope amplitude during MQL-CO grinding. This was attributed to the minimal impact of temper damage on the newly formed surface grains at higher work $f = 12 \text{ m/min}$ , hindering magnetic domain wall rotation.

### 3.2. Non-Conventional Manufacturing (NCM)

#### 3.2.1. Electrical Discharge Machining (EDM)

EDM is an unconventional machining process that uses the induced thermal energy leading to material ablation. Electrical discharges remove material from a wrought stock that develops high-energy plasma at  $T$  between 8000 °C and 20,000 °C, melting material and vaporizing cavities from an electrode [141]. The main advantage of this NCM process is the ability to machine materials with high hardness without needing contact between the tool and the workpiece [142]. The main drawbacks are the relatively slow material removal and energy intensity [143]. Micro-EDM is particularly useful to machine CuBe alloys, which are known for their toxicity and high mechanical strength [144]. These alloys have a higher  $k$ , which can enhance the thermal removal of unwanted material [145,146]. Table 14 addresses some of the most recent state-of-the-art works regarding EDM AMPCO<sup>®</sup>, INVAR-36<sup>®</sup>, and HT steels.

**Table 14.** EDM processes: addressed challenges and remarks.

Material	Author	Challenges	Remarks
AMPCO <sup>®</sup>	Yıldız et al. [147]	The thickness ( $t$ ) of the white layer (WLT) that forms during the EDD of the CuBe alloy and how the WLT changes as the drilling depth increases were examined. Statistical analysis using ANOVA and significant difference methods determined that as the drilling depth, working current, and pulse duration increase, $t$ the WLT also increases.	The working current, pulse-on time ( $T_{on}$ ), and pulse-off time ( $T_{off}$ ) duration primarily influence the WLT formed during the process. The depth of the drilled hole also plays a meaningful role. A second-order response surface model has been created in this study, incorporating the main and interaction effects of various influential combinations of EDD control factors and variations in hole measurements, effectively predicting the formation of the WLT's $t$ and optimal EDD performance with a 95% confidence interval. For thinner $t$ achievement, using lower working currents, $T_{on}$ and $T_{off}$ are recommended during EDD. The authors address that future attempts should address the variations in $R_a$ that arise due to the EDD machining depth.
	Dong et al. [144]	In this investigation, auxiliary electrodes were employed to mitigate the impacts of stray-current corrosion on the terminal surfaces of holes in the C17200 [26] CuBe alloy. Micro-EDM was utilized as a safe and efficient machining process for working with CuBe alloys, notwithstanding their toxic properties and mechanical robustness.	The micro-EDM drilling of micro-holes on the C17200 CuBe alloy in deionized H <sub>2</sub> O reveals electrochemical dissolution and anodic oxidation occurring at the end surface of the micro-hole, directly impacting the performance and lifespan of components. The effectiveness of micro-EDM with an auxiliary electrode in mitigating stray-current corrosion on the C17200 CuBe alloy was confirmed across various pulse currents and pulse widths. Fine micro-hole end surfaces were achieved with the auxiliary electrode under 0.34 A pulse current conditions and a 20 μs pulse width. Minimal impact on electrode wear was verified with the auxiliary electrode. However, the machining time slightly increased when the pulse current was below 0.55 A and the pulse width was 20 μs. Beyond this threshold, the effect of the auxiliary electrode on machining time was less apparent.
	Rebelo et al. [148]	This work presented an experiment that examines how various processing parameters for the rough, finishing, and micro-finishing or polishing of EDM impact the MRR and surface quality when machining high-strength CuBe alloys.	(1) The average recrystallization rates observed in the CuBe alloy are approximately 0.1 of those in steels. (2) The average peak of the recrystallization rate is achieved at shorter on-times than that of steels, and the maximum of the curves shifted towards lower discharge times. (3) In rough regimes: $T_{on} = 50 \mu s$ , while in finish regimes: $T_{on} = 12.8 \mu s$ .

Table 14. Cont.

Material	Author	Challenges	Remarks
	Mouralova et al. [143]	This work aimed to optimize AMPCOLOY® 35 EDM parameters such as $V_c$ , surface topography, and complex surface. A mathematical model was developed to determine the optimal $V_c$ , and an optimization process was carried out using this model. The optimization aimed to achieve the maximum $V_c$ while minimizing $R_a$ . Equal importance was given to both objectives during the optimization procedure.	All the machined samples exhibited a similar surface morphology, regardless of the specific machine parameters used. The samples were relatively smooth and did not contain any large craters. While there were some small cracks on the surface of all samples, these were found to be purely superficial and did not extend into the cross-section of the samples. This evidence suggested that the cracks did not compromise the functionality or service life of the machined parts. The machined specimens' surfaces display segregated lead crystals in various regions. The subsurface region of all samples was entirely free of defects, and the recast layer was thin, measuring no more than $t = 15 \mu\text{m}$ and only present in localized areas. Using TEM, a lamella analysis identified an elevated concentration of alloying elements in the recast layer. The analysis also revealed a shift in crystal orientation resulting from Wire EDM (WEDM)
AMPCO®	Mouralova et al. [149]	These authors developed mathematical models to optimize the machining process of AMPCOLOY® 35 across a varying $t$ , ranging from 5 mm to 160 mm in increments of 5 mm, employing WEDM to enhance the surface characteristics of mould parts. The Box–Behnken-type experiment design generated 448 samples.	<p>(1) The highest <math>R_a = 4 \mu\text{m}</math> at the centre of the samples was reported, while a slightly lower value of <math>R_a = 3.6 \mu\text{m}</math> was observed at the margins. The lowest <math>R_a = 1.6 \mu\text{m}</math> was recorded in the sample machined with <math>T_{\text{on}} = 6 \mu\text{s}</math>, <math>T_{\text{off}} = 40 \mu\text{s}</math>, and a peak current (<math>I_p</math>) of 25 A.</p> <p>(2) All examined factors demonstrated positive main effects, increasing, with the interaction between <math>T_{\text{off}}</math> and <math>I_p</math> being the most influential.</p> <p>(3) Consistent with expectations, the sample with <math>t = 5 \text{ mm}</math> exhibited the highest Wire Feed rate (WF) of 20.24 mm/min.</p> <p>(4) <math>T_{\text{on}}</math> and <math>I_p</math> positively impact <math>V_c</math>, while <math>T_{\text{off}}</math> had a detrimental effect.</p> <p>(5) Upon analysis, no discernible defects were detected in the surface morphology of the samples. Minor discrepancies between the centres and margins of the samples were observed in the size and articulation of the craters, aligning closely with the topographic analysis.</p>
	Dong et al. [150]	The mill micro-ball socket technique in the C17200 [26] CuBe alloy was introduced using micro-EDM. Specifically, a linear compensation method for the tool electrode was employed, and a variable $t$ approach was proportional to the desired outcome. The machining parameters were analysed to attain superior dimensional accuracy in producing micro-ball sockets.	<p>The most favourable outcomes were obtained when <math>k = 0.98</math> and the initial layer was <math>t = 0.024 \text{ mm}</math> (innovative approach for manufacturing micro-ball sockets in C17200 [26]).</p> <p>When comparing constant <math>t</math> approaches, it was found that implementing a proportional variable <math>t</math> layered technique could significantly decrease the error rate during machining. This effect was particularly evident when the number of layers was slightly increased. The time required for machining decreased as the initial <math>t</math> of the material increased.</p> <p>Based on the evaluation of the shape precision of micro-ball sockets, an initial layer <math>t = 0.024 \text{ mm}</math> was recommended as an ideal starting point for micro-EDM milling. This approach should be implemented alongside a linear compensation of the tool electrode and a proportional variable <math>t</math> method, with a <math>k = 0.98</math>, for ideal results.</p>

Table 14. Cont.

Material	Author	Challenges	Remarks
INVAR-36®	Mohanty et al. [146]	These authors systematically refined multiple input parameters for the wire EDM machining of INVAR-36®, employing TGRA for optimization. Key control parameters, including $T_{on}$ , pulse-off time ( $T_{off}$ ), servo voltage ( $SV$ ), and $WF$ , were selected to assess their impact on the MRR and SR of the INVAR-36® alloy. To achieve the optimization of the MRR and SR, a total of nine experiments were conducted using the $L_9$ orthogonal array design.	The MRR increases with a higher $WF$ and $T_{on}$ , with $SV$ demonstrating the most negligible impact on the MRR, contributing only 16.22%. The optimal combination of process parameters for achieving the maximum MRR comprises $T_{on} = 25 \mu s$ , $T_{off} = 46 \mu s$ , $WF = 5 \text{ mm/min}$ , and $SV = 30 \text{ V}$ . The SR escalates with elevations in $WF$ and $T_{off}$ , while $SV$ exhibits minimal influence on SR, contributing only 17.97%. The ideal set of process parameters for attaining the lowest SR involves $T_{on} = 25 \mu s$ , $T_{off} = 19 \mu s$ , $WF = 3 \text{ mm/min}$ , and $SV = 20 \text{ V}$ . $WF$ emerges as the most influential parameter affecting the MRR and SR, whereas $SV$ is the least influential factor in both aspects.
HT Steels	Gill and Kumar [151]	The surface alloying phenomenon induced by the EDM process employing tool electrodes fabricated via powder metallurgy (PM) was explored. The study employed a TGRA with an $L_{18}$ orthogonal array to determine the optimal setup for achieving the minimum SR. Experiments were conducted on the AISI H11 (DIN 1.2343) hot die steel utilizing WCu electrodes produced via the PM process. Tool polarity ( $P$ ), the percentage of the alloying element in the tool (%W), $I_p$ , $T_{on}$ , duty factor ( $\tau$ ), and $SV$ input parameters were considered, and their significance was analysed through ANOVA. Scanning Electron Microscopy (SEM), Energy-Dispersive Spectroscopy (EDS), and X-ray diffraction (XRD) were utilized to examine the characteristics of the machined surface.	The presence of $W_3C$ on the surface suggests a reaction between $W$ migrated from the PM tool and $C$ in the high- $T$ discharge zone. A portion of $Cu$ from the PM electrode is also transferred to the machined surface. As $Cu$ forms a solid solution with the $\alpha$ -Fe phase, this phenomenon further enhances the machined surface quality and the hardness by up to 83%. This improves the surface to abrasion, extending the lifespan of press tools and dies for hot working applications. No microcracks are observed on surfaces machined with the PM tool, indicating that the alloying process does not compromise SR, which is $R_a \approx 4 \mu m$ and aligns with typical values obtained in conventional EDM processes. The optimal parameters for SR are $P+$ , the tool with 10%W, $I_p = 5 \text{ A}$ , $T_{on} = 100 \mu s$ , $\tau = 64\%$ , and $SV = 30 \text{ V}$ , and the optimal parameters for microhardness enhancement are $P+$ , the tool with 15%W, $I_p = 15 \text{ A}$ , $T_{on} = 200 \mu s$ , $\tau = 64\%$ , and $SV = 50 \text{ V}$ .
	Hess et al. [152]	During the process of the AISI H11 (DIN 1.2343) EDM, the application of thermal energy leads to the formation of microstructural changes and modifications in the material of the machined component. Although a $T$ near or above the evaporation point is generated during the discharge at the surface, the actual $T$ decreases as the depth within the component increases.	Ablation occurs when the material is exposed to thermal loads caused by an electrical discharge, which results in the heating of the material to $T$ , exceeding the melting and evaporation points. As a result of the structural changes occurring within the component during EDM, the material properties are modified, leading to significant impacts on the functionality and potential applications of the resulting manufactured part. The degree of austenitization became progressively less advanced, further moving deeper inside the workpiece. At the top of the material, the carbides wholly dissolved during the heating process, but as they moved towards the bottom of the heat-affected zone (HAZ), some carbides remained even after the heating process. When the $T$ gradients and maximum temperature ( $T_{max}$ ) are increased, the areas of retained austenite become larger.

Table 14. Cont.

Material	Author	Challenges	Remarks
HT Steels	Le [153]	The impact of various main process parameters, such as peak current ( $I_p$ ) and pulse-on time ( $T_{on}$ ) during fine finishing, as well as powder concentration ( $C_p$ ), on the machined performance (MP) and recast layer properties (RLPs) of AISI H13 (DIN 1.2344) steel samples was studied in this work. The goal was to investigate how these parameters affect the quality of the finished product.	As the main process parameters are incrementally changed, both the MRR and TWR show an upward trend. There is a decrease in the percentage of the Fe element on the surface of the recast layer compared to the substrate of AISI H13 steel. While the percentage of C increases compared to the substrate layer, it remains lower than the percentage found on the surface of the recast layer in the EDM process.

### 3.2.2. Laser Beam Drilling (LBD)

LBD, a non-contact drilling process derived from Laser Beam Machining (LBM) [154], shares similar operational principles but offers distinct advantages. It enables the precise and accurate drilling of holes at high speeds and efficiency across various materials such as metals, ceramics, plastics, and composites. Additionally, it can create holes with high aspect ratios, increased tapers [155], and intricate geometries while minimizing thermal damage and surface defects. Furthermore, LDM boasts a higher MRR than electroerosion techniques in manufacturing applications [141]. Table 15 addresses some of the most recent state-of-the-art works regarding LDM, INVAR-36<sup>®</sup>, and HT steels.

Table 15. LDM processes: addressed challenges and remarks.

Material	Author	Challenges	Remarks
INVAR-36 <sup>®</sup>	Butkus et al. [156]	A burst mode laser was used to perform micromachining on 20–250 $\mu\text{m}$ thick INVAR-36 <sup>®</sup> foils to determine the best micromachining parameters for percussion drilling. The method used for drilling holes involved firing multiple laser pulses transversely onto the sample, known as percussion drilling, without moving the beam. The study examined the rate at which holes were drilled and how the quality of the holes was affected by the number of laser pulses per burst and the laser's average power.	The micromachining efficiency significantly improved using the burst mode laser. The micromachining throughput was up to 10 $\times$ higher when using the burst mode. Using a specific laser mode of repetition rate burst can enhance the efficiency of micromachining through holes. The efficiency of ablation decreases as the $t$ of the sample increases. The efficiency of ablation decreases for thick samples. In general, generating burst pulses for micromachining appears to be a promising approach to achieve faster and more efficient results while maintaining a similar level of quality.
	Hauschwitz et al. [58]	Choose INVAR-36 <sup>®</sup> for high-quality micrometre-scale patterns within metal shadow masks, like OLED displays, because of its exceptional characteristics, precisely its low $k$ .	The optical module's attributes enable the rapid alignment of the setup to achieve a consistent intensity distribution throughout the entire pattern and facilitate focus adjustments. Through the identification of the ablation edge, optimal pulse counts, and fluence levels, a suitable processing range can be determined to achieve effective, high-quality drilling and cutting with minimal heat-affected zones.
	Chung et al. [157]	An ultrashort pulsed laser system was highly recommended for micro-hole drilling in INVAR-36 <sup>®</sup> , as it minimized the adverse effects of heat and produced high-quality edges.	An Nd:YAG laser is the preferred method to create a hole in INVAR-36 <sup>®</sup> . Although it has the drawback of producing burrs at the edges that necessitate further processing, the study decided to employ an ultrashort pulsed laser instead. As the pulse energy increased, the area removed during the ablation of INVAR-36 <sup>®</sup> reached a point of gradual stabilization.

Table 15. Cont.

Material	Author	Challenges	Remarks
INVAR-36 <sup>®</sup>	Choi et al. [158]	The impact of focal plane adjustments, achieved through vibration, on the quality of the INVAR-36 <sup>®</sup> alloy's fabrication during femtosecond laser hole drilling was examined. This process is used to create high-quality metal masks. The ability to control the taper angles during femtosecond laser hole drilling makes it a promising technique for the accurate micromachining of various intelligent devices.	The processing efficiency and productivity were maximized when the initial laser pulse was directed towards the sample's upper surface, resulting in the most profound processed depth. Therefore, synchronizing the laser and vibrator in the hole processing system can significantly impact overall productivity. Decreasing the vibrator amplitude during femtosecond laser hole machining increased the taper angle of the processed hole. These findings indicate that the hole's taper angle can be effectively managed by adjusting the amplitude of the continuously operating vibrator.
HT Steels	Rubaiee [159]	The authors LDMed a 0.44 mm thick AISI H13 (DIN 1.2344) using 100 m fibre laser beams. The Complex Proportional Assessment (COPRAS) method optimizes the fibre laser settings for drilling holes. ANOVA was conducted to validate the model, and ANN was utilized to forecast the experimental outcomes.	Laser power emerges as the most critical factor influencing the quality of drilled holes. Under the optimal setup, the drilled holes exhibit $Ra = 4.27 \mu\text{m}$ , a heat-affected zone of $89.89 \mu\text{m}$ , and an overcut of $139.60 \mu\text{m}$ . The experimental results indicate a close match between the observed and predicted values, and the optimal conditions yield a superior surface precision compared to the initial trials.

#### 4. Discussion

Given all the information presented in this document, a SWOT analysis was performed to discuss the perceptions of the AMPCO<sup>®</sup>, INVAR-36<sup>®</sup>, and HT steels' machinability among the various manufacturing processes addressed. The AMPCO<sup>®</sup>, INVAR-36<sup>®</sup>, and HT steels' machinability analysis is divided into milling (Table 16), turning (Table 17), drilling (Table 18), surface polishing (Table 19), EDM (Table 20), and LDM (Table 21).

Table 16. SWOT analysis on machinability of injection mould materials' milling.

	Positive Factors	Negative Factors
	<b>Strengths</b>	
textInternal factors	<b>High MRR:</b> Milling processes, especially optimized, can achieve a high MRR, allowing for efficient material removal, which is particularly advantageous for large-scale production.	<b>Weakness</b>
	<b>Surface Finish Improvement:</b> By selecting optimal parameters, milling operations can yield an improved surface finish, enhancing the quality and appearance of the final products.	
	<b>Adaptability:</b> Milling processes can be adapted to various materials, including AMPCO <sup>®</sup> , INVAR-36 <sup>®</sup> , and HT steels, showcasing versatility in machining different injection mould materials.	
	<b>TW Mechanism Understanding:</b> Extensive research has provided insights into the TW mechanisms during milling, enabling a better understanding and management of tool longevity and performance.	
		<b>SR Variation:</b> Achieving consistent surface finish across different materials and machining conditions can be challenging, leading to SR variations and impacting part quality.
		<b>TW:</b> Especially in HSM operations, it can lead to reduced TL and decreased machining accuracy over time.
		<b>Challenges with AM Preforms:</b> The machining of additively manufactured preforms, such as WAAM INVAR-36 <sup>®</sup> , presents inherent challenges like warping, internal stresses, and porosities, affecting machining accuracy and surface finish.

Table 16. Cont.

	Positive Factors	Negative Factors
	<p><b>Opportunities</b></p> <p><b>Advanced Coatings:</b> The integration of advanced coatings, such as TiAlTiN, can enhance tool performance and prolong tool life, offering opportunities for improved efficiency and cost savings in milling operations.</p> <p><b>Optimization Techniques:</b> Advanced optimization techniques like Taguchi methods and response surface analysis (RSA) can help identify optimal milling parameters, maximizing the MRR and surface finish while minimizing TW.</p> <p><b>Application in Various Industries:</b> The versatility of milling processes makes them applicable across diverse industries, including aerospace, automotive, and manufacturing, offering opportunities for market expansion and growth.</p>	<p><b>Threats</b></p> <p><b>Material Complexity:</b> Machining AMPCO®, INVAR-36®, and HT steels require precision and expertise due to their unique material properties, posing challenges in achieving desired machining outcomes.</p> <p><b>Environmental Concerns:</b> HSM operations may consume significant energy and produce waste, raising environmental concerns.</p> <p><b>Competitive Landscape:</b> The milling industry faces competition from alternative machining methods and emerging technologies, which may offer more efficient or cost-effective solutions, posing a threat to traditional milling processes.</p>
External factors		

Table 17. SWOT analysis on machinability of injection mould materials' turning.

	Positive Factors	Negative Factors
	<p><b>Strengths</b></p> <p><b>Advanced Tool Coatings:</b> Utilization of advanced tool coatings such as TiCN-Al<sub>2</sub>O<sub>3</sub>-TiN and TiCN enhances wear resistance and improves tool lifespan, contributing to efficient machining of materials like AMPCO®, INVAR-36®, and HT steels.</p> <p><b>Optimized Cutting Parameters:</b> Studies have developed mathematical models and response surface methodologies to determine optimal cutting parameters, leading to improved MRR and surface finish, particularly in turning of INVAR-36® and hardened steels.</p> <p><b>Hardness Enhancement:</b> Cryogenic treatment of cutting tools increases hardness and wear resistance, resulting in prolonged TL and enhanced surface finish, especially when machining materials like AISI H11 steel.</p> <p><b>TW Mechanism Analysis:</b> In-depth investigations into mechanisms of TW, including abrasion, diffusion, and oxidation, provide insights into performance of cutting tools when turning AMPCO®, INVAR-36®, and HT steels, facilitating better tool selection and process optimization.</p>	<p><b>Weakness</b></p> <p><b>High TW Rate:</b> Materials like CuBe alloys exhibit high rates of TW, leading to increased SR and decreased TL, which may pose challenges in achieving desired machining outcomes.</p> <p><b>Limited TL:</b> Despite advancements in tool coatings and treatments, certain materials, such as CuBe alloys, may still result in significant TW and reduced TL, impacting machining efficiency and cost-effectiveness.</p>
Internal factors		
	<p><b>Opportunities</b></p> <p><b>Further Research and Development:</b> Continued research into advanced tool materials, coatings, and cutting strategies can lead to more robust cutting tools tailored for specific materials like AMPCO®, INVAR-36®, and HT steels, enhancing machining efficiency and quality.</p> <p><b>Process Optimization:</b> Optimization of cutting parameters and tool geometries based on comprehensive studies can further improve material removal rates, surface finish, and tool lifespan, offering opportunities for enhanced productivity and cost savings in machining operations.</p>	<p><b>Threats</b></p> <p><b>Material Complexity:</b> Materials like CuBe alloys with hard particles embedded within them pose challenges in machining due to their complex microstructures and high TW rates, potentially leading to increased TW and reduced machining efficiency.</p> <p><b>Tool Degradation:</b> Despite advancements in tool coatings and treatments, factors such as high <math>V_c</math> and <math>f</math> can still lead to rapid tool degradation and reduced tool performance, posing challenges in maintaining consistent machining quality and productivity.</p>
External factors		

**Table 18.** SWOT analysis on machinability of injection mould materials' drilling.

		Positive Factors	Negative Factors
		Strengths	Weakness
Internal factors		<p><b>Advanced Coated Drills:</b> Utilization of advanced PVD TiAlN-coated drills enhances wear resistance and prolongs tool lifespan, contributing to efficient drilling of materials like INVAR-36<sup>®</sup>, particularly in multi-material stacks.</p> <p><b>In-depth Phenomena Analysis:</b> Studies have provided insights into crucial cutting phenomena such as thrust forces, <math>T_{cut}</math>, and chip formation during drilling operations, aiding in understanding challenges associated with drilling materials like INVAR-36<sup>®</sup>.</p>	<p><b>Challenging Material Properties:</b> Materials like INVAR-36<sup>®</sup> pose challenges in drilling operations due to their high plasticity, toughness, and low <math>k</math>, leading to increased <math>T_{cut}</math> and chip adhesion, which may impact drilling performance and tool lifespan.</p> <p><b>Complex TW Mechanisms:</b> Drilling multi-layered claddings and materials with varying microstructural features induces complex TW mechanisms, including adhesion, coating peeling, and BUE formation, which may affect drilling quality and tool integrity.</p>
		<p><b>Opportunities</b></p> <p><b>Optimized Laser Cladding Parameters:</b> Further research into laser cladding parameters, such as powder sizes and power, can optimize material properties and microstructural features, potentially reducing TW and improving drilling quality for materials like AISI H13 tool steel.</p> <p><b>Enhanced Tool Coatings:</b> Development of advanced coatings and treatments for drill bits tailored to specific properties of AMPCO<sup>®</sup>, INVAR-36<sup>®</sup>, and HT steels can improve wear resistance and tool lifespan, offering opportunities for more efficient drilling operations.</p>	<p><b>Threats</b></p> <p><b>Increased TW:</b> Drilling operations involving materials like INVAR-36<sup>®</sup> and multi-layered claddings may increase TW due to high <math>T_{cut}</math> and chip adhesion, posing challenges in maintaining drilling performance and tool integrity.</p> <p><b>Quality Control Challenges:</b> Ensuring drilling quality and dimensional accuracy of drilled holes in materials with complex microstructural features may be challenging, particularly in multi-material stacks or laser-clad components, where variations in material properties can impact drilling performance and hole quality.</p>
External factors			

**Table 19.** SWOT analysis on machinability of injection mould materials' surface polishing.

		Positive Factors	Negative Factors
		Strengths	Weakness
Internal factors		<p><b>Advanced Electrochemical Techniques:</b> The use of advanced electrochemical methods, such as electropolishing with an Ethaline electrolyte, offers efficient surface polishing solutions for materials like AMPCO<sup>®</sup> 22 and AMPCO<sup>®</sup> 712, resulting in significant reductions in SR and an improved corrosion resistance.</p> <p><b>Innovative Numerical Investigations:</b> Numerical investigations provide insights into the nano-polishing characteristics of materials like INVAR-36<sup>®</sup>, helping to understand the primary factors influencing surface quality and guiding the development of effective polishing strategies.</p>	<p><b>Complex Surface Interactions:</b> The surface polishing of materials like INVAR-36<sup>®</sup> and AISI H11 tool steel involves complex interactions between polishing parameters, material properties, and tooling, leading to challenges in achieving desired surface finishes without introducing subsurface damage or compromising material integrity.</p> <p><b>Dependence on Process Parameters:</b> Surface polishing techniques, such as laser polishing, are highly dependent on accurate process parameters, and deviations from optimal conditions can result in variations in surface quality, microstructural characteristics, and mechanical properties, impacting the overall polishing effectiveness.</p>
		<p><b>Opportunities</b></p> <p><b>Multi-Step Polishing Techniques:</b> Multi-step laser polishing offers opportunities to tailor surface properties and microstructural characteristics, enabling the production of surfaces with an enhanced hardness, reduced SR, and improved microstructural integrity.</p> <p><b>Non-Destructive Evaluation Methods:</b> Integrating non-destructive evaluation methods, such as MBN, provides opportunities to assess the surface quality, detect defects, and evaluate material characteristics without compromising the integrity of the polished surface, enhancing quality control and process monitoring capabilities.</p>	<p><b>Threats</b></p> <p><b>Surface Damage and Defects:</b> Surface polishing processes may inadvertently introduce surface defects, such as subsurface damage, thermal damage, or oxidation layers, particularly in materials like hardened AISI H13 die steel, posing challenges in achieving the desired surface quality and integrity.</p> <p><b>Environmental Impact:</b> Surface polishing techniques, especially those involving traditional lubrication fluids or abrasive materials, may pose environmental risks due to the generation of waste products or the use of potentially hazardous chemicals, necessitating sustainable and eco-friendly polishing alternatives to mitigate environmental impact.</p>
External factors			

**Table 20.** SWOT analysis on machinability of injection mould materials' EDM.

	Positive Factors	Negative Factors
	<b>Strengths</b>	
Internal factors	<p><b>Process Optimization:</b> Research studies have developed mathematical models and conducted optimization procedures to enhance EDM parameters for materials like AMPCOLOY® 35 and INVAR-36®, leading to an improved machining efficiency, surface quality, and dimensional accuracy.</p> <p><b>Surface Alloying:</b> The EDM process with PM tool electrodes has shown the potential for surface alloying, enhancing surface properties such as hardness and abrasion resistance, which can extend the lifespan of injection mould components made from materials like AISI H11 and other HT steels.</p> <p><b>Microstructural Modifications:</b> EDM induces microstructural changes in materials like AISI H11 steel, leading to modifications that can enhance material properties and functionality, offering opportunities for tailored material characteristics in injection mould applications.</p>	<p><b>Weakness</b></p> <p><b>Surface Defects:</b> EDM processes may result in surface defects such as cracks, craters, or recast layers, particularly when machining materials like CuBe alloys, posing challenges in achieving desired surface quality and integrity.</p> <p><b>Complex Parameter Interactions:</b> The interaction between EDM parameters, such as pulse current, pulse duration, and electrode composition, can be complex, making it challenging to optimize machining processes effectively and consistently.</p>
	<b>Opportunities</b>	<b>Threats</b>
	External factors	<p><b>Optimization and Process Control:</b> Continued research into EDM parameters and process optimization techniques, such as response surface modelling and statistical analysis, presents opportunities to improve machining efficiency, enhance surface quality, and minimize defects for AMPCO®, INVAR-36®, and HT steels.</p> <p><b>Innovative Machining Strategies:</b> Exploring EDM techniques, such as auxiliary electrodes, variable <i>t</i> approaches, and PM tool electrodes, offers opportunities to mitigate process challenges, improve dimensional accuracy, and enhance SR for PIM.</p>

**Table 21.** SWOT analysis on machinability of injection mould materials' LBD.

	Positive Factors	Negative Factors
	<b>Strengths</b>	
Internal factors	<p><b>High Precision Machining:</b> LBD offers exceptional precision, allowing for the creation of micro-holes and intricate patterns with minimal heat-affected zones, making it suitable for manufacturing intricate components used in injection moulds.</p> <p><b>Versatility in Material Compatibility:</b> LBD can be effectively applied to a wide range of materials, including AMPCO®, INVAR-36®, and HT steels, due to its ability to adjust parameters such as pulse energy and repetition rate to match the specific material properties.</p>	<p><b>Weakness</b></p> <p><b>Surface Quality Considerations:</b> Despite its precision, LBD may produce burrs or heat-affected zones, particularly in HT steels, which could require additional post-processing steps to achieve the desired surface quality.</p> <p><b>Complex Process Optimization:</b> Optimizing LBD parameters, such as pulse energy, repetition rate, and focal plane adjustments, can be challenging and require thorough experimentation and analysis to achieve optimal results for different materials and hole geometries.</p>

Table 21. Cont.

	Positive Factors	Negative Factors
External factors	<p><b>Opportunities</b></p> <p><b>Advanced Laser Technologies:</b> Continual advancements in laser technologies, such as ultrashort pulsed and burst mode lasers, offer opportunities to enhance drilling efficiency, reduce heat-affected zones, and improve surface quality for INVAR-36<sup>®</sup> and HT steels.</p> <p><b>Process Control and Automation:</b> Integrating advanced control systems and automation technologies can streamline LBD processes, increase productivity, and ensure consistent quality in producing injection mould components.</p>	<p><b>Threats</b></p> <p><b>Material-Specific Challenges:</b> Each material, including INVAR-36<sup>®</sup> and HT steels, presents unique challenges during LBD, such as variations in thermal conductivity and susceptibility to heat-induced defects, which may limit process capabilities and require tailored machining strategies.</p> <p><b>Cost and Equipment Requirements:</b> LBD equipment and maintenance costs can be significant, particularly for advanced laser systems, which may pose a barrier to entry for small-scale manufacturers or those with limited resources.</p>

## 5. Conclusions

The main objective of this review was to provide a concise and comprehensive review of the most recent investigations of these alloys' manufacturing processes. The machinability of AMPCO<sup>®</sup>, INVAR-36<sup>®</sup>, and HT steel challenges from other authors were presented, remarks were highlighted, and their objectives and conclusions were discussed. In the context of milling, turning, drilling, surface polishing, EDM, and LBD, the following conclusions can be drawn:

- Both AMPCO<sup>®</sup> and HT steels exhibit good machinability characteristics in milling and turning processes, allowing for an efficient MRR and dimensional accuracy,
- INVAR-36<sup>®</sup> presents challenges due to its low  $k$  and tendency to generate heat during machining, requiring the careful selection of cutting parameters to avoid TW and surface defects,
- The drillability of AMPCO<sup>®</sup> is generally favourable, with optimal cutting parameters leading to efficient hole production and minimal TW,
- INVAR-36<sup>®</sup> poses challenges in drilling due to its high plasticity and toughness, leading to increased thrust forces and  $T_{cut}$ ,
- The surface polishing of AMPCO<sup>®</sup> and INVAR-36<sup>®</sup> can be effectively achieved using techniques such as electropolishing and nano-polishing, enhancing surface quality and corrosion resistance,
- HT steels may require additional post-machining processes to achieve the desired surface finishes, depending on the specific material characteristics and machining parameters,
- EDM proves to be a versatile machining technique for all three addressed alloys, offering high precision and complex shape capabilities,
- Challenges include the formation of surface defects and recast layers, particularly in HT steels, requiring careful process optimization and control,
- LBD demonstrates high efficiency and precision in drilling micro-holes in materials like INVAR-36<sup>®</sup>, with techniques such as burst mode and ultrashort pulsed lasers yielding promising results,
- The optimization of laser parameters is crucial for achieving the desired drilling quality while minimizing heat-affected zones and surface defects.

As for limitations, it was difficult to obtain information, particularly regarding the conventional drilling and LBD of AMPCO<sup>®</sup> alloys and AISI L6 (DIN 1.2714). This hiatus of the literature highlights the need for further research and development in these areas. On the other hand, a trend in EDM drilling was seen for CuBe alloys compared to traditional drilling. Regarding prospects, there is a clear need for more research and development on the CuBe alloys, as this topic remains relatively underdeveloped. Moreover, there is a scarcity of information regarding the composition and research of the alloy, emphasizing

that it is a heavily commercial branded material and the importance of further exploration in this field. Overall, this review article sheds light on the current state of CM and NCM processes applied to the HPIM moulding industry. Each machining technique offers unique advantages and challenges, and it is intended to bring significant contributions to the endeavours of the HPIM industry, particularly concerning the milling of AMPCO<sup>®</sup>, INVAR-36<sup>®</sup>, and HT steels. Continued research and innovation in machining technologies will further enhance the capabilities of these techniques for manufacturing injection moulding materials.

**Author Contributions:** Conceptualization: F.R.N., A.F.V.P., F.J.G.S. and R.D.S.G.C.; methodology: F.R.N., A.F.V.P., F.J.G.S. and R.D.S.G.C.; validation: N.P.V.S., R.D.F.S.C., M.L.S.B. and R.C.M.S.-C.; formal analysis: N.P.V.S., R.D.F.S.C., M.L.S.B. and R.C.M.S.-C.; investigation: F.R.N. and A.F.V.P.; data curation: N.P.V.S., R.D.F.S.C., M.L.S.B. and R.C.M.S.-C.; writing—original draft preparation: A.F.V.P.; writing—review and editing: F.J.G.S., R.D.S.G.C. and R.C.M.S.-C.; visualization: N.P.V.S., R.D.F.S.C., M.L.S.B. and R.C.M.S.-C.; supervision: F.J.G.S. and R.D.S.G.C.; project administration: F.J.G.S.; funding acquisition: F.J.G.S. All authors have read and agreed to the published version of the manuscript.

**Funding:** The work was developed under the “DRIVOLUTION—Transition to the factory of the future”, with the reference DRIVOLUTION C644913740-00000022 research project, supported by European Structural and Investments Funds with the “Portugal2020” program scope.

**Data Availability Statement:** No new data were created or analyzed in this study. Data sharing is not applicable to this article.

**Acknowledgments:** The authors thank ISEP, INEGI, and CIDEM for their institutional support.

**Conflicts of Interest:** The authors declare no conflicts of interest.

## References

1. Silva, F.J.G.; Martinho, R.P.; Alexandre, R.J.D.; Baptista, A.P.M. Increasing the wear resistance of molds for injection of glass fiber reinforced plastics. *Wear* **2011**, *271*, 2494–2499. [[CrossRef](#)]
2. Martinho, R.P.; Silva, F.J.; Alexandre, R.J.; Baptista, A.P. TiB<sub>2</sub> nanostructured coating for GFRP injection moulds. *J. Nanosci. Nanotechnol.* **2011**, *11*, 5374–5382. [[CrossRef](#)] [[PubMed](#)]
3. Arruda, É.M.; de Paiva, A.P.; Brandão, L.C.; Ferreira, J.R. Robust optimisation of surface roughness of AISI H13 hardened steel in the finishing milling using ball nose end mills. *Precis. Eng.* **2019**, *60*, 194–214. [[CrossRef](#)]
4. Park, S.J.; Lee, J.H.; Yang, J.; Heogh, W.; Kang, D.; Yeon, S.M.; Kim, S.H.; Hong, S.; Son, Y.; Park, J. Lightweight injection mold using additively manufactured Ti-6Al-4V lattice structures. *J. Manuf. Process.* **2022**, *79*, 759–766. [[CrossRef](#)]
5. Silva, F.J.G.; Martinho, R.P.; Baptista, A.P.M. Characterization of laboratory and industrial CrN/CrCN/diamond-like carbon coatings. *Thin Solid Film.* **2014**, *550*, 278–284. [[CrossRef](#)]
6. Nunes, V.; Silva, F.J.G.; Andrade, M.F.; Alexandre, R.; Baptista, A.P.M. Increasing the lifespan of high-pressure die cast molds subjected to severe wear. *Surf. Coat. Technol.* **2017**, *332*, 319–331. [[CrossRef](#)]
7. Pinto, H.; Silva, F.J.G. Optimisation of Die Casting Process in Zamak Alloys. *Procedia Manuf.* **2017**, *11*, 517–525. [[CrossRef](#)]
8. Pinto, H.A.; Silva, F.J.G.; Martinho, R.P.; Campilho, R.D.S.G.; Pinto, A.G. Improvement and validation of Zamak die casting moulds. *Procedia Manuf.* **2019**, *38*, 1547–1557. [[CrossRef](#)]
9. Almeida, F.d.; Sousa, V.F.C.; Silva, F.J.G.; Campilho, R.D.S.G.; Ferreira, L.P. Development of a Novel Design Strategy for Moving Mechanisms Used in Multi-Material Plastic Injection Molds. *Appl. Sci.* **2021**, *11*, 11805. [[CrossRef](#)]
10. Penne, R.; Silva, F.; Campilho, R.; Santos, G.; Sousa, V.; Ferreira, L.; Sá, J.; Pereira, M. A new approach to increase the environmental sustainability of the discharging process in the over-injection of conduits for bowden cables using automation. *Proc. Inst. Mech. Eng. Part C J. Mech. Eng. Sci.* **2022**, *236*, 8823–8833. [[CrossRef](#)]
11. Ellingsen, D.G.; Møller, L.B.; Aaseth, J. Chapter 35—Copper. In *Handbook on the Toxicology of Metals*, 4th ed.; Nordberg, G.F., Fowler, B.A., Nordberg, M., Eds.; Academic Press: San Diego, CA, USA, 2015; pp. 765–786.
12. Freudenberger, J.; Tikana, L.; Hosford, W.F. Alloys: Copper. In *Encyclopedia of Condensed Matter Physics*, 2nd ed.; Chakraborty, T., Ed.; Academic Press: Oxford, UK, 2024; pp. 601–634.
13. ASM International. *Surface Engineering*; ASM International: West Conshohocken, PA, USA, 1994.
14. Sousa, V.F.C.; Castanheira, J.; Silva, F.J.G.; Fecheira, J.S.; Pinto, G.; Baptista, A. Wear Behavior of Uncoated and Coated Tools in Milling Operations of AMPCO (Cu-Be) Alloy. *Appl. Sci.* **2021**, *11*, 7762. [[CrossRef](#)]
15. Jacquet, P.A. Electrolytic Method for obtaining Bright Copper Surfaces. *Nature* **1935**, *135*, 1076. [[CrossRef](#)]
16. Hoar, T.P.; Rothwell, G.P. The influence of solution flow on anodic polishing. Copper in aqueous o-phosphoric acid. *Electrochim. Acta* **1964**, *9*, 135–150. [[CrossRef](#)]

17. Jakubowski, M.; Pałczyński, C. Chapter 30—Beryllium. In *Handbook on the Toxicology of Metals*, 4th ed.; Nordberg, G.F., Fowler, B.A., Nordberg, M., Eds.; Academic Press: San Diego, CA, USA, 2015; pp. 635–653.
18. Zou, Y.; Chen, G.; Ren, C.; Ge, J.; Qin, X. Performance and mechanism of hole-making of CFRP/Ti-6Al-4V stacks using ultrasonic vibration helical milling process. *Int. J. Adv. Manuf. Technol.* **2021**, *117*, 3529–3547. [[CrossRef](#)]
19. Wang, Z.; Kovvuri, V.R.; Araujo, A.C.; Bacci Da Silva, M.; Hung, N.; Bukkapatnam, S. Built-up-edge effects on surface deterioration in micromilling processes. *J. Manuf. Process.* **2016**, *24*, 321–327. [[CrossRef](#)]
20. Zitoune, R.; Krishnaraj, V.; Sofiane Almabouacif, B.; Collombet, F.; Sima, M.; Jolin, A. Influence of machining parameters and new nano-coated tool on drilling performance of CFRP/Aluminium sandwich. *Compos. Part B Eng.* **2012**, *43*, 1480–1488. [[CrossRef](#)]
21. Ozcatalbas, Y. Chip and built-up edge formation in the machining of in situ Al4C3–Al composite. *Mater. Des.* **2003**, *24*, 215–221. [[CrossRef](#)]
22. Campbell, F.C. Chapter 3—Magnesium and Beryllium. In *Manufacturing Technology for Aerospace Structural Materials*; Campbell, F.C., Ed.; Elsevier Science: Oxford, UK, 2006; pp. 93–118.
23. Crone, W.C. Compositional variation and precipitate structures of copper–beryllium single crystals grown by the Bridgman technique. *J. Cryst. Growth* **2000**, *218*, 381–389. [[CrossRef](#)]
24. Prashanth Reddy, K.; Panitapu, B. High thermal conductivity mould insert materials for cooling time reduction in thermoplastic injection moulds. *Mater. Today Proc.* **2017**, *4*, 519–526. [[CrossRef](#)]
25. Zhong, Z.W.; Leong, M.H.; Liu, X.D. The wear rates and performance of three mold insert materials. *Mater. Des.* **2011**, *32*, 643–648. [[CrossRef](#)]
26. *ASTM B 194-15*; Standard Specification for Copper-Beryllium Alloy Plate, Sheet, Strip, and Rolled Bar. ASTM International: West Conshohocken, PA, USA, 2015.
27. Tan, C.; Zhou, K.; Ma, W.; Min, L. Interfacial characteristic and mechanical performance of maraging steel-copper functional bimetal produced by selective laser melting based hybrid manufacture. *Mater. Des.* **2018**, *155*, 77–85. [[CrossRef](#)]
28. Cunha, A.; Marques, A.; Silva, F.S.; Gasik, M.; Trindade, B.; Carvalho, O.; Bartolomeu, F. 420 stainless steel-Cu parts fabricated using 3D Multi-Material Laser Powder Bed Fusion: A new solution for plastic injection moulds. *Mater. Today Commun.* **2022**, *32*, 103852. [[CrossRef](#)]
29. Huzaim, N.H.M.; Rahim, S.Z.A.; Musa, L.; Abdellah, A.E.-h.; Abdullah, M.M.A.B.; Rennie, A.; Rahman, R.; Garus, S.; Bloch, K.; Sandu, A.V.; et al. Potential of Rapid Tooling in Rapid Heat Cycle Molding: A Review. *Materials* **2022**, *15*, 3725. [[CrossRef](#)]
30. Baragetti, S.; Terranova, A.; Vimercati, M. Friction behaviour evaluation in beryllium–copper threaded connections. *Int. J. Mech. Sci.* **2009**, *51*, 790–796. [[CrossRef](#)]
31. Sharma, A.; Joshi, S.S.; Datta, D.; Balasubramaniam, R. Modeling and analysis of tool wear mechanisms in diamond turning of copper beryllium alloy. *J. Manuf. Process.* **2020**, *56*, 439–450. [[CrossRef](#)]
32. Ramesh, B.; Venkatesh, R.; Abraham, D.; Clement, S.; Ronadson, B.; Elayaperumal, A. Optimization of Process Parameter Levels during Conventional Milling of Beryllium Copper Alloy Using End Mill. *Int. J. Adv. Res. Sci. Eng.* **2013**, *1*, 57–63.
33. Avelar-Batista Wilson, J.C.; Banfield, S.; Eichler, J.; Leyland, A.; Matthews, A.; Housden, J. An investigation into the tribological performance of Physical Vapour Deposition (PVD) coatings on high thermal conductivity Cu-alloy substrates and the effect of an intermediate electroless Ni–P layer prior to PVD treatment. *Thin Solid Film.* **2012**, *520*, 2922–2931. [[CrossRef](#)]
34. Nogueira, F.R.; Pedroso, A.F.V.; Silva, F.J.G.; Campilho, R.D.S.G.; Sales-Contini, R.C.M.; Sebbe, N.P.V.; Casais, R.C.B. A Comparative Study on the Wear Mechanisms of Uncoated and TiAlTaN-Coated Tools Used in Machining AMPCO® Alloy. *Coatings* **2024**, *14*, 4. [[CrossRef](#)]
35. Durocher, A.; Lipa, M.; Chappuis, P.; Schlosser, J.; Huber, T.; Schedler, B. TORE SUPRA experience of copper chromium zirconium electron beam welding. *J. Nucl. Mater.* **2002**, *307–311*, 1554–1557. [[CrossRef](#)]
36. Lipa, M.; Durocher, A.; Tivey, R.; Huber, T.; Schedler, B.; Weigert, J. The use of copper alloy CuCrZr as a structural material for actively cooled plasma facing and in vessel components. *Fusion Eng. Des.* **2005**, *75–79*, 469–473. [[CrossRef](#)]
37. Nogueira, F.R.; Pedroso, A.F.V.; Sousa, V.F.C.; Sebbe, N.P.V.; Sales-Contini, R.C.M.; Barbosa, M.L.S. A Brief Review of Injection-Mould Materials Hybrid Manufacturing Processes. In *Intelligent Manufacturing: Establishing Bridges for More Sustainable Manufacturing Systems*; Springer: Cham, Switzerland, 2024; pp. 796–806.
38. Butterworth, G.J.; Forty, C.B.A. A survey of the properties of copper alloys for use as fusion reactor materials. *J. Nucl. Mater.* **1992**, *189*, 237–276. [[CrossRef](#)]
39. Rouxel, B.; Mischler, S.; Logé, R.; Igual Munoz, A. Wear behaviour of novel copper alloy as an alternative to copper-beryllium. *Wear* **2023**, *524*, 204817. [[CrossRef](#)]
40. Cacciamani, G.; Dinsdale, A.; Palumbo, M.; Pasturel, A. The Fe–Ni system: Thermodynamic modelling assisted by atomistic calculations. *Intermetallics* **2010**, *18*, 1148–1162. [[CrossRef](#)]
41. Li, G.; Gao, M.; Chen, C.; Zhang, C.; Zeng, X. Characterisation comparison of laser and laser–arc hybrid welding of Invar 36 alloy. *Sci. Technol. Weld. Join.* **2014**, *19*, 30–37. [[CrossRef](#)]
42. *ASTM F 1684-06 (2016)*; Standard Specification for Iron-Nickel and Iron-Nickel-Cobalt Alloys for Low Thermal Expansion Applications. ASTM International: West Conshohocken, PA, USA, 2016.
43. Guillaume, C.E. Invar and Its Applications. *Nature* **1904**, *71*, 134–139. [[CrossRef](#)]
44. Sahoo, A.; Medicherla, V.R.R. Fe-Ni Invar alloys: A review. *Mater. Today Proc.* **2021**, *43*, 2242–2244. [[CrossRef](#)]

45. Rancourt, D.G.; Hargraves, P.; Lamarche, G.; Dunlap, R.A. Microstructure and low temperature magnetism of Fe-Ni invar alloys. *J. Magn. Magn. Mater.* **1990**, *87*, 71–82. [[CrossRef](#)]
46. Wei, K.; Yang, Q.; Ling, B.; Yang, X.; Xie, H.; Qu, Z.; Fang, D. Mechanical properties of Invar 36 alloy additively manufactured by selective laser melting. *Mater. Sci. Eng. A* **2020**, *772*, 138799. [[CrossRef](#)]
47. van Schilfgaarde, M.; Abrikosov, I.A.; Johansson, B. Origin of the Invar effect in iron–nickel alloys. *Nature* **1999**, *400*, 46–49. [[CrossRef](#)]
48. Kanca, Y. Microstructural characterization and dry sliding wear behavior of boride layers grown on Invar-36 superalloy. *Surf. Coat. Technol.* **2022**, *449*, 128973. [[CrossRef](#)]
49. Song, S.H.; Yuan, Z.X.; Jia, J.; Shen, D.D.; Guo, A.M. The role of tin in the hot-ductility deterioration of a low-carbon steel. *Metall. Mater. Trans. A* **2003**, *34*, 1611–1616. [[CrossRef](#)]
50. Abbasi, S.M.; Morakabati, M.; Mahdavi, R.; Momeni, A. Effect of microalloying additions on the hot ductility of cast FeNi36. *J. Alloys Compd.* **2015**, *639*, 602–610. [[CrossRef](#)]
51. Wang, B.; Guo, Y.; Zhang, Z.; Yi, X.; Wang, D. Investigation of cryogenic friction and wear properties of Invar 36 alloy against Si<sub>3</sub>N<sub>4</sub> ceramic balls. *Wear* **2023**, *518–519*, 204648. [[CrossRef](#)]
52. Erden, F.; Akgul, B.; Danaci, I.; Oner, M.R. Thermoelectric and thermomechanical properties of invar 36: Comparison with common thermoelectric materials. *J. Alloys Compd.* **2023**, *932*, 167690. [[CrossRef](#)]
53. Zheng, S.; Sokoluk, M.; Yao, G.; de Rosa, I.; Li, X. Fe–Ni Invar alloy reinforced by WC nanoparticles with high strength and low thermal expansion. *SN Appl. Sci.* **2019**, *1*, 172. [[CrossRef](#)]
54. Yakout, M.; Elbestawi, M.A.; Veldhuis, S.C. Density and mechanical properties in selective laser melting of Invar 36 and stainless steel 316L. *J. Mater. Process. Technol.* **2019**, *266*, 397–420. [[CrossRef](#)]
55. Wang, Q.; Shen, J.; Hu, S.; Zhao, G.; Zhou, J. Microstructure and Mechanical Properties of Fe-36Ni and 304L Dissimilar Alloy Lap Joints by Pulsed Gas Tungsten Arc Welding. *Materials* **2020**, *13*, 4016. [[CrossRef](#)] [[PubMed](#)]
56. Aldalur, E.; Suárez, A.; Veiga, F. Thermal expansion behaviour of Invar 36 alloy parts fabricated by wire-arc additive manufacturing. *J. Mater. Res. Technol.* **2022**, *19*, 3634–3645. [[CrossRef](#)]
57. Zhan, X.; Liu, X.; Wei, Y.; Chen, J.; Chen, J.; Liu, H. Microstructure and property characteristics of thick Invar alloy plate joints using weave bead welding. *J. Mater. Process. Technol.* **2017**, *244*, 97–105. [[CrossRef](#)]
58. Hauschwitz, P.; Stoklasa, B.; Kuchařík, J.; Turčičová, H.; Písařík, M.; Brajer, J.; Rostohar, D.; Mocek, T.; Duda, M.; Lucianetti, A. Micromachining of Invar with 784 Beams Using 1.3 ps Laser Source at 515 nm. *Materials* **2020**, *13*, 2962. [[CrossRef](#)]
59. Akca, E.; Gürsel, A. A Review on Superalloys and IN718 Nickel-Based INCONEL Superalloy. *Period. Eng. Nat. Sci. (PEN)* **2015**, *3*. [[CrossRef](#)]
60. Rath, N.; Kumar, P.; Kumar khatkar, S.; Gupta, A. Non-conventional machining of nickel based superalloys: A review. *Mater. Today Proc.* **2023**, *in press*. [[CrossRef](#)]
61. Qiu, C.; Chen, H.; Liu, Q.; Yue, S.; Wang, H. On the solidification behaviour and cracking origin of a nickel-based superalloy during selective laser melting. *Mater. Charact.* **2019**, *148*, 330–344. [[CrossRef](#)]
62. Yang, Q.; Wei, K.; Yang, X.; Xie, H.; Qu, Z.; Fang, D. Microstructures and unique low thermal expansion of Invar 36 alloy fabricated by selective laser melting. *Mater. Charact.* **2020**, *166*, 110409. [[CrossRef](#)]
63. Kim, Y.-K.; Park, S.-H.; Lee, K.-A. Effect of post-heat treatment on the thermophysical and compressive mechanical properties of Cu-Ni-Sn alloy manufactured by selective laser melting. *Mater. Charact.* **2020**, *162*, 110194. [[CrossRef](#)]
64. Koga, N.; Nameki, T.; Umezawa, O.; Tschan, V.; Weiss, K.-P. Tensile properties and deformation behavior of ferrite and austenite duplex stainless steel at cryogenic temperatures. *Mater. Sci. Eng. A* **2021**, *801*, 140442. [[CrossRef](#)]
65. Park, M.; Park, G.-W.; Kim, S.-h.; Choi, Y.-W.; Kim, H.C.; Kwon, S.-H.; Noh, S.; Jeon, J.B.; Kim, B.J. Tensile and Charpy impact properties of heat-treated high manganese steel at cryogenic temperatures. *J. Nucl. Mater.* **2022**, *570*, 153982. [[CrossRef](#)]
66. Soares, J.P. *Aços—Características e Tratamentos*, 6th ed.; Publindústria, Produção de Comunicação Lda.: Porto, Portugal, 2010.
67. Podgornik, B.; Žužek, B.; Kafexhiu, F.; Leskovšek, V. Effect of Si Content on Wear Performance of Hot Work Tool Steel. *Tribol. Lett.* **2016**, *63*, 5. [[CrossRef](#)]
68. Huber, F.; Bischof, C.; Hentschel, O.; Heberle, J.; Zettl, J.; Nagulin, K.Y.; Schmidt, M. Laser beam melting and heat-treatment of 1.2343 (AISI H11) tool steel—Microstructure and mechanical properties. *Mater. Sci. Eng. A* **2019**, *742*, 109–115. [[CrossRef](#)]
69. Outeiro, J.C. 11—Residual stresses in machining. In *Mechanics of Materials in Modern Manufacturing Methods and Processing Techniques*; Silberschmidt, V.V., Ed.; Elsevier: Amsterdam, The Netherlands, 2020; pp. 297–360.
70. Salem, M.; Le Roux, S.; Dour, G.; Lamesle, P.; Choquet, K.; Rézai-Aria, F. Effect of aluminizing and oxidation on the thermal fatigue damage of hot work tool steels for high pressure die casting applications. *Int. J. Fatigue* **2019**, *119*, 126–138. [[CrossRef](#)]
71. Sun, Y.; Wang, J.; Li, M.; Wang, Y.; Li, C.; Dai, T.; Hao, M.; Ding, H. Thermal and mechanical properties of selective laser melted and heat treated H13 hot work tool steel. *Mater. Des.* **2022**, *224*, 111295. [[CrossRef](#)]
72. Lee, H.T.; Liu, C. Optimizing the EDM hole-drilling strain gage method for the measurement of residual stress. *J. Mater. Process. Technol.* **2009**, *209*, 5626–5635. [[CrossRef](#)]
73. Mishigdorzhyn, U.; Semenov, A.; Ulakhanov, N.; Milonov, A.; Dashev, D.; Gulyashinov, P. Microstructure and Wear Resistance of Hot-Work Tool Steels after Electron Beam Surface Alloying with B4C and Al. *Lubricants* **2022**, *10*, 90. [[CrossRef](#)]
74. Casteletti, L.C.; Lombardi, A.N.; Totten, G.E. Boriding. In *Encyclopedia of Tribology*; Wang, Q.J., Chung, Y.-W., Eds.; Springer: Boston, MA, USA, 2013; pp. 249–255.

75. Podgornik, B.; Sedlaček, M.; Žužek, B.; Guštin, A. Properties of Tool Steels and Their Importance When Used in a Coated System. *Coatings* **2020**, *10*, 265. [[CrossRef](#)]
76. Pérez, M.; Rodríguez, C.; Belzunce, F.J. The Use of Cryogenic Thermal Treatments to Increase the Fracture Toughness of a Hot Work Tool Steel Used to Make Forging Dies. *Procedia Mater. Sci.* **2014**, *3*, 604–609. [[CrossRef](#)]
77. Sánchez-Huerta, D.; López-Perrusquia, N.; García, E.; Hilerio-Cruz, I.; Flores-Martínez, M.; Doñu-Ruiz, M.A.; Muhl, S. Micro-abrasive wear behavior by the ball cratering technique on AISI L6 steel for agricultural application. *Mater. Lett.* **2021**, *283*, 128904. [[CrossRef](#)]
78. Koniorczyk, P.; Zieliński, M.; Sienkiewicz, J.; Zmywaczyk, J.; Dębski, A. Experimental Studies of Thermophysical Properties and Microstructure of X37CrMoV5-1 Hot-Work Tool Steel and Maraging 350 Steel. *Materials* **2023**, *16*, 1206. [[CrossRef](#)] [[PubMed](#)]
79. Dandekar, T.R.; Khatirkar, R.K. Structural and wear assessment of H11 die steel as a function of tempering temperature. *Mater. Today Proc.* **2023**, in press. [[CrossRef](#)]
80. Balaško, T.; Vončina, M.; Burja, J.; Šetina Batič, B.; Medved, J. High-Temperature Oxidation Behaviour of AISI H11 Tool Steel. *Metals* **2021**, *11*, 758. [[CrossRef](#)]
81. Riccardo, G.; Rivolta, B.; Gorla, C.; Concli, F. Cyclic behavior and fatigue resistance of AISI H11 and AISI H13 tool steels. *Eng. Fail. Anal.* **2021**, *121*, 105096. [[CrossRef](#)]
82. Fonseca, E.B.; Gabriel, A.H.G.; Araújo, L.C.; Santos, P.L.L.; Campo, K.N.; Lopes, E.S.N. Assessment of laser power and scan speed influence on microstructural features and consolidation of AISI H13 tool steel processed by additive manufacturing. *Addit. Manuf.* **2020**, *34*, 101250. [[CrossRef](#)]
83. Katoch, S.; Sehgal, R.; Singh, V. Wear behavior of differently cryogenically treated AISI H13 steel against cold work steel. *Proc. Inst. Mech. Eng. Part E J. Process Mech. Eng.* **2018**, *233*, 292–305. [[CrossRef](#)]
84. Łukaszewicz, G.; Tacikowski, M.; Kulka, M.; Chmielarz, K.; Węsierska-Hinca, M.; Świątnicki, W.A. Effect of Prior Boriding on Microstructure and Mechanical Properties of Nanobainitic X37CrMoV5-1 Hot-Work Tool Steel. *Materials* **2023**, *16*, 4237. [[CrossRef](#)]
85. *ISO 4957:2018*; Tool Steels. International Organization for Standardization: Geneva, Switzerland, 2018; p. 33.
86. Lysykh, S.; Kornopoltsev, V.; Mishigdorzhyn, U.; Kharaev, Y.; Xie, Z. Evaluation of Wear Resistance of AISI L6 and 5140 Steels after Surface Hardening with Boron and Copper. *Lubricants* **2023**, *11*, 48. [[CrossRef](#)]
87. Twardowski, P.; Wojciechowski, S.; Wieczorowski, M.; Mathia, T. Surface roughness analysis of hardened steel after high-speed milling. *Scanning* **2011**, *33*, 386–395. [[CrossRef](#)]
88. Liao, Y.; Deschamps, F.; Loures, E.d.F.R.; Ramos, L.F.P. Past, present and future of Industry 4.0—A systematic literature review and research agenda proposal. *Int. J. Prod. Res.* **2017**, *55*, 3609–3629. [[CrossRef](#)]
89. Azarian, M.; Yu, H.; Shiferaw, A.T.; Stevik, T.K. Do We Perform Systematic Literature Review Right? A Scientific Mapping and Methodological Assessment. *Logistics* **2023**, *7*, 89. [[CrossRef](#)]
90. Tóth, Á.; Suta, A.; Pimentel, J.; Argoti, A. A comprehensive, semi-automated systematic literature review (SLR) design: Application to P-graph research with a focus on sustainability. *J. Clean. Prod.* **2023**, *415*, 137741. [[CrossRef](#)]
91. Sousa, V.F.C.; Silva, F.J.G. Recent Advances on Coated Milling Tool Technology—A Comprehensive Review. *Coatings* **2020**, *10*, 235. [[CrossRef](#)]
92. Lim, S.C.; Lim, C.Y.H. Effective use of coated tools—The wear-map approach. *Surf. Coat. Technol.* **2001**, *139*, 127–134. [[CrossRef](#)]
93. Lakner, T.; Bergs, T.; Döbbeler, B. Additively manufactured milling tool with focused cutting fluid supply. *Procedia CIRP* **2019**, *81*, 464–469. [[CrossRef](#)]
94. Kovacevic, R.; Cherukuthota, C.; Mohan, R. Improving Milling Performance with High Pressure Waterjet Assisted Cooling/Lubrication. *J. Eng. Ind.* **1995**, *117*, 331–339. [[CrossRef](#)]
95. Groover, M.P. *Fundamentals of Modern Manufacturing: Materials, Processes, and Systems*; Wiley: Hoboken, NJ, USA, 2019; p. 816.
96. da Silva, L.R.; dos Santos, F.V.; de Moraes, H.L.O.; Calado, C.R. Evaluation of the use of vegetable oils in the grinding of AISI 4340 steel. *Int. J. Adv. Manuf. Technol.* **2022**, *120*, 499–514. [[CrossRef](#)]
97. Zuo, J.; Lin, Y.; He, M. An Investigation of the Adhesive Effect on the Flank Wear Properties of a WC/Co-based TiAlN-Coated Tool for Milling a Be/Cu Alloy. *Metals* **2019**, *9*, 444. [[CrossRef](#)]
98. Sousa, V.F.C.; Da Silva, F.J.G.; Pinto, G.F.; Baptista, A.; Alexandre, R. Characteristics and Wear Mechanisms of TiAlN-Based Coatings for Machining Applications: A Comprehensive Review. *Metals* **2021**, *11*, 260. [[CrossRef](#)]
99. Sousa, V.F.C.; Fernandes, F.; Silva, F.J.G.; Costa, R.D.F.S.; Sebbe, N.; Sales-Contini, R.C.M. Wear Behavior Phenomena of TiN/TiAlN HiPIMS PVD-Coated Tools on Milling Inconel 718. *Metals* **2023**, *13*, 684. [[CrossRef](#)]
100. Zuo, J.; Lin, Y.; Zheng, J.; Zhong, P.; He, M. An investigation of thermal-mechanical interaction effect on PVD coated tool wear for milling Be/Cu alloy. *Vacuum* **2019**, *167*, 271–279. [[CrossRef](#)]
101. Baptista, A.; Silva, F.J.G.; Porteiro, J.; Míguez, J.L.; Pinto, G.; Fernandes, L. On the Physical Vapour Deposition (PVD): Evolution of Magnetron Sputtering Processes for Industrial Applications. *Procedia Manuf.* **2018**, *17*, 746–757. [[CrossRef](#)]
102. Martinho, R.P.; Silva, F.J.G.; Martins, C.; Lopes, H. Comparative study of PVD and CVD cutting tools performance in milling of duplex stainless steel. *Int. J. Adv. Manuf. Technol.* **2019**, *102*, 2423–2439. [[CrossRef](#)]
103. Zheng, X.; Ying, G.; Chen, Y.; Fu, Y. The Effects of Cutting Parameters on Work-Hardening of Milling Invar 36. *Adv. Mater. Res.* **2015**, *1089*, 373–376. [[CrossRef](#)]
104. Cornelius, A.; Jacobs, L.; Lamsey, M.; McNeil, L.; Hamel, W.; Schmitz, T. Hybrid manufacturing of Invar mold for carbon fiber layup using structured light scanning. *Manuf. Lett.* **2022**, *33*, 133–142. [[CrossRef](#)]

105. Gil Del Val, A.; Cearsolo, X.; Suarez, A.; Veiga, F.; Altuna, I.; Ortiz, M. Machinability characterization in end milling of Invar 36 fabricated by wire arc additive manufacturing. *J. Mater. Res. Technol.* **2023**, *23*, 300–315. [[CrossRef](#)]
106. Singh, P.K.; Saini, P.; Kumar, D. Multi response optimization of CNC end milling of AISI H11 alloy steel for rough and finish machining using TGRA. *Mater. Today Proc.* **2020**, *26*, 2564–2573. [[CrossRef](#)]
107. Şahinoğlu, A. Investigation of machinability properties of AISI H11 tool steel for sustainable manufacturing. *Proc. Inst. Mech. Eng. Part E J. Process Mech. Eng.* **2022**, *236*, 2717–2728. [[CrossRef](#)]
108. Martinho, R.P.; Silva, F.J.G.; Baptista, A.P.M. Cutting forces and wear analysis of Si<sub>3</sub>N<sub>4</sub> diamond coated tools in high speed machining. *Vacuum* **2008**, *82*, 1415–1420. [[CrossRef](#)]
109. Silva, F.J.G.; Martinho, R.P.; Martins, C.; Lopes, H.; Gouveia, R.M. Machining GX2CrNiMoN26-7-4 DSS Alloy: Wear Analysis of TiAlN and TiCN/Al<sub>2</sub>O<sub>3</sub>/TiN Coated Carbide Tools Behavior in Rough End Milling Operations. *Coatings* **2019**, *9*, 392. [[CrossRef](#)]
110. Platt, T.; Baumann, J.; Biermann, D. Potential of high-feed milling structured dies for material flow control in hot forming. *Prod. Eng.* **2023**, *17*, 463–471. [[CrossRef](#)]
111. Wojciechowski, S.; Krajewska-Śpiewak, J.; Maruda, R.W.; Krolczyk, G.M.; Nieslony, P.; Wieczorowski, M.; Gawlik, J. Study on ploughing phenomena in tool flank face—workpiece interface including tool wear effect during ball-end milling. *Tribol. Int.* **2023**, *181*, 108313. [[CrossRef](#)]
112. ISO 8688-2:1989; Tool Life Testing in Milling—Part 2: End Milling. International Organization for Standardization: Geneva, Switzerland, 1989; p. 26.
113. Abu Bakar, H.N.; Ghani, J.A.; Haron, C.H.C.; Ghazali, M.J.; Kasim, M.S.; Al-Zubaidi, S.; Jouini, N. Wear mechanisms of solid carbide cutting tools in dry and cryogenic machining of AISI H13 steel with varying cutting-edge radius. *Wear* **2023**, *523*, 204758. [[CrossRef](#)]
114. Grum, J.; Kisin, M. Influence of microstructure on surface integrity in turning—Part II: The influence of a microstructure of the workpiece material on cutting forces. *Int. J. Mach. Tools Manuf.* **2003**, *43*, 1545–1551. [[CrossRef](#)]
115. Grum, J.; Kisin, M. The influence of the microstructure of three Al–Si alloys on the cutting-force amplitude during fine turning. *Int. J. Mach. Tools Manuf.* **2006**, *46*, 769–781. [[CrossRef](#)]
116. Abrikosov, I.A.; Kissavos, A.E.; Liot, F.; Alling, B.; Simak, S.I.; Peil, O.; Ruban, A.V. Competition between magnetic structures in the Fe rich fcc FeNi alloys. *Phys. Rev. B* **2007**, *76*, 014434. [[CrossRef](#)]
117. Warren, A.W.; Guo, Y.B. Characteristics of Residual Stress Profiles in Hard Turned Versus Ground Surfaces with and without a White Layer. *J. Manuf. Sci. Eng.* **2009**, *131*, 041004. [[CrossRef](#)]
118. Meyer, R.; Köhler, J.; Denkena, B. Influence of the tool corner radius on the tool wear and process forces during hard turning. *Int. J. Adv. Manuf. Technol.* **2012**, *58*, 933–940. [[CrossRef](#)]
119. Tönshoff, H.K.; Arendt, C.; Amor, R.B. Cutting of Hardened Steel. *CIRP Ann.* **2000**, *49*, 547–566. [[CrossRef](#)]
120. Crangle, J.; Hallam, G.C. The Magnetization of Face-Centred Cubic and Body-Centred Cubic Iron + Nickel Alloys. *Proc. R. Soc. London. Ser. A Math. Phys. Sci.* **1963**, *272*, 119–132.
121. Sharma, A.; Datta, D.; Balasubramaniam, R. An investigation of tool and hard particle interaction in nanoscale cutting of copper beryllium. *Comput. Mater. Sci.* **2018**, *145*, 208–223. [[CrossRef](#)]
122. Zhao, G.; Huang, C.; He, N.; Liu, H.; Zou, B. Preparation and cutting performance of reactively hot pressed TiB<sub>2</sub>-SiC ceramic tool when machining Invar36 alloy. *Int. J. Adv. Manuf. Technol.* **2016**, *86*, 2679–2688. [[CrossRef](#)]
123. Mahir, A. A Comparative Study on the Cutting Performance of Uncoated, AlTiN and TiCN-Al<sub>2</sub>O<sub>3</sub> Coated Carbide Inserts in Turning of Invar 36 Alloy. *J. Eng. Res. Appl. Sci.* **2022**, *11*, 2045–2061.
124. Suresh, R.; Basavarajappa, S. Effect of Process Parameters on Tool Wear and Surface Roughness during Turning of Hardened Steel with Coated Ceramic Tool. *Procedia Mater. Sci.* **2014**, *5*, 1450–1459. [[CrossRef](#)]
125. Benlahmidi, S.; Aouici, H.; Boutaghane, F.; Khellaf, A.; Fnides, B.; Yallese, M.A. Design optimization of cutting parameters when turning hardened AISI H11 steel (50 HRC) with CBN7020 tools. *Int. J. Adv. Manuf. Technol.* **2017**, *89*, 803–820. [[CrossRef](#)]
126. Liu, J.; Ji, X.; Guo, Z.; Qin, C.; Xiao, Y.; You, Q. Characteristics and cutting performance of the CVD coatings on the TiCN-based cermets in turning hardened AISI H13 steel. *J. Mater. Res. Technol.* **2020**, *9*, 1389–1399. [[CrossRef](#)]
127. Özbek, N.A. Effects of cryogenic treatment types on the performance of coated tungsten tools in the turning of AISI H11 steel. *J. Mater. Res. Technol.* **2020**, *9*, 9442–9456. [[CrossRef](#)]
128. Binali, R.; Kuntoğlu, M.; Pimenov, D.Y.; Ali Usca, Ü.; Kumar Gupta, M.; Erdi Korkmaz, M. Advance monitoring of hole machining operations via intelligent measurement systems: A critical review and future trends. *Measurement* **2022**, *201*, 111757. [[CrossRef](#)]
129. Ortner, M.; Kromoser, B. Influence of different parameters on drilling forces in automated drilling of concrete with industrial robots. *Autom. Constr.* **2023**, *150*, 104814. [[CrossRef](#)]
130. Ficici, F. Investigation of wear mechanism in drilling of PPA composites for automotive industry. *J. Eng. Res.* **2023**, *11*, 100034. [[CrossRef](#)]
131. Ma, L.; Ma, Z.; Yu, H.; Li, S.; Pang, M.; Wang, Z. Experimental Investigation of Thrust Force in the Drilling of Titanium Alloy Using Different Machining Techniques. *Metals* **2022**, *12*, 1905. [[CrossRef](#)]
132. Li, S.; Wang, Y.; Wu, H.; Liu, L. Dynamic response of drill string when sonic drilling rig is applied to blasting hole operation. *Geoenergy Sci. Eng.* **2023**, *221*, 211392. [[CrossRef](#)]
133. Zhang, H.; Dang, J.; An, Q.; Cai, X.; Chen, M. Study on the drilling performances of a newly developed CFRP/invar co-cured material. *J. Manuf. Process.* **2021**, *66*, 669–678. [[CrossRef](#)]

134. Sorgato, M.; Bertolini, R.; Ghiotti, A.; Bruschi, S. Tool wear assessment when drilling AISI H13 tool steel multilayered claddings. *Wear* **2023**, *524–525*, 204853. [[CrossRef](#)]
135. Bhattacharyya, B.; Doloi, B. Chapter Eight—Advanced finishing processes. In *Modern Machining Technology*; Bhattacharyya, B., Doloi, B., Eds.; Academic Press: Cambridge, MA, USA, 2020; pp. 675–743.
136. Darvell, B.W. Chapter 20—Cutting, Abrasion and Polishing. In *Materials Science for Dentistry*, 10th ed.; Darvell, B.W., Ed.; Woodhead Publishing: Sawston, UK, 2018; pp. 515–539.
137. Kityk, A.A.; Danilov, F.I.; Protsenko, V.S.; Pavlik, V.; Boča, M.; Halahovets, Y. Electropolishing of two kinds of bronze in a deep eutectic solvent (Ethaline). *Surf. Coat. Technol.* **2020**, *397*, 126060. [[CrossRef](#)]
138. Wang, W.; Hua, D.; Luo, D.; Zhou, Q.; Eder, S.J.; Li, S.; Wang, Z.; Wang, H. Exploring the nano-polishing mechanisms of Invar. *Tribol. Int.* **2022**, *175*, 107840. [[CrossRef](#)]
139. Temmler, A.; Liu, D.; Preußner, J.; Oeser, S.; Luo, J.; Poprawe, R.; Schleifenbaum, J.H. Influence of laser polishing on surface roughness and microstructural properties of the remelted surface boundary layer of tool steel H11. *Mater. Des.* **2020**, *192*, 108689. [[CrossRef](#)]
140. Awale, A.S.; Srivastava, A.; Kumar, A.; Yusufzai, M.Z.K.; Vashista, M. Magnetic non-destructive evaluation of microstructural and mechanical characteristics of hardened AISI H13 die steel upon sustainable grinding. *J. Manuf. Process.* **2023**, *103*, 193–206. [[CrossRef](#)]
141. Pedroso, A.F.V.; Sebbe, N.P.V.; Silva, F.J.G.; Campilho, R.D.S.G.; Sales-Contini, R.C.M.; Martinho, R.P.; Casais, R.B. An In-Depth Exploration of Unconventional Machining Techniques for INCONEL<sup>®</sup> Alloys. *Materials* **2024**, *17*, 1197. [[CrossRef](#)] [[PubMed](#)]
142. Kliuev, M.; Florio, K.; Akbari, M.; Wegener, K. Influence of energy fraction in EDM drilling of Inconel 718 by statistical analysis and finite element crater-modelling. *J. Manuf. Process.* **2019**, *40*, 84–93. [[CrossRef](#)]
143. Mouralova, K.; Beneš, L.; Prokes, T.; Bednar, J.; Zahradnicek, R.; Jankovych, R.; Fries, J.; Vontor, J. Analysis of the Machinability of Copper Alloy Ampcoloy by WEDM. *Materials* **2020**, *13*, 893. [[CrossRef](#)]
144. Dong, S.; Wang, Z.; Wang, Y. Research on micro-EDM with an auxiliary electrode to suppress stray-current corrosion on C17200 beryllium copper alloy in deionized water. *Int. J. Adv. Manuf. Technol.* **2017**, *93*, 857–867. [[CrossRef](#)]
145. Ho, K.H.; Newman, S.T. State of the art electrical discharge machining (EDM). *Int. J. Mach. Tools Manuf.* **2003**, *43*, 1287–1300. [[CrossRef](#)]
146. Mohanty, A.; Mohapatra, R.; Das, S.P. Optimization of Wire EDM Process Parameters for Machining of INVAR 36 Alloy. In *Proceedings of the Advances in Materials Processing and Manufacturing Applications*, Jaipur, India, 5–6 November 2020; pp. 1–11.
147. Yıldız, Y.; Sundaram, M.; Rajurkar, K. Empirical modeling of the white layer thickness formed in electrodischarge drilling of beryllium–copper alloys. *Int. J. Adv. Manuf. Technol.* **2012**, *66*, 1745–1755. [[CrossRef](#)]
148. Rebelo, J.C.; Morão Dias, A.; Mesquita, R.; Vassalo, P.; Santos, M. An experimental study on electro-discharge machining and polishing of high strength copper–beryllium alloys. *J. Mater. Process. Technol.* **2000**, *103*, 389–397. [[CrossRef](#)]
149. Mouralova, K.; Bednar, J.; Benes, L.; Prokes, T.; Zahradnicek, R.; Fries, J. Mathematical Models for Machining Optimization of Ampcoloy 35 with Different Thicknesses Using WEDM to Improve the Surface Properties of Mold Parts. *Materials* **2023**, *16*, 100. [[CrossRef](#)]
150. Dong, S.; Ji, H.; Zhou, J.; Li, X.; Ding, L.; Wang, Z. Fabrication of Micro-Ball Sockets in C17200 Beryllium Copper Alloy by Micro-Electrical Discharge Machining Milling. *Materials* **2023**, *16*, 323. [[CrossRef](#)] [[PubMed](#)]
151. Gill, A.S.; Kumar, S. Surface alloying of H11 die steel by tungsten using EDM process. *Int. J. Adv. Manuf. Technol.* **2015**, *78*, 1585–1593. [[CrossRef](#)]
152. Hess, R.; Grethe, P.; Heidemanns, L.; Herrig, T.; Klink, A.; Bergs, T. Simulation based derivation of changed rim zone properties caused by thermal loadings during EDM process. *Procedia CIRP* **2022**, *113*, 41–46. [[CrossRef](#)]
153. Le, V.T. An investigation on machined performance and recast layer properties of AISI H13 steel by Powder Mixed-EDM in fine-finishing process. *Mater. Chem. Phys.* **2022**, *276*, 125362. [[CrossRef](#)]
154. Mahbub, M.R.; Rashid, A.; Jahan, M.P. Chapter 8—Hybrid machining and finishing processes. In *Advanced Machining and Finishing*; Gupta, K., Pramanik, A., Eds.; Elsevier: Amsterdam, The Netherlands, 2021; pp. 287–338.
155. Alsorujji, G.; Muthuramalingam, T.; Moustafa, E.B.; Elsheikh, A. Investigation and TGRA based optimization of laser beam drilling process during machining of Nickel Inconel 718 alloy. *J. Mater. Res. Technol.* **2022**, *18*, 720–730. [[CrossRef](#)]
156. Butkus, S.; Jukna, V.; Paipulas, D.; Barkauskas, M.; Sirutkaitis, V. Micromachining of Invar Foils with GHz, MHz and kHz Femtosecond Burst Modes. *Micromachines* **2020**, *11*, 733. [[CrossRef](#)] [[PubMed](#)]
157. Chung, I.L.Y.; Kim, J.-D.; Kang, K.-H. Ablation drilling of invar alloy using ultrashort pulsed laser. *Int. J. Precis. Eng. Manuf.* **2009**, *10*, 11–16. [[CrossRef](#)]

158. Choi, W.; Kim, H.Y.; Jeon, J.W.; Chang, W.S.; Cho, S.-H. Vibration-Assisted Femtosecond Laser Drilling with Controllable Taper Angles for AMOLED Fine Metal Mask Fabrication. *Materials* **2017**, *10*, 212. [[CrossRef](#)]
159. Rubaiee, S. Parametric assessment of surface behavior and the impact of heat in micro drilling of fiber laser machined AISI h13. *Proc. Inst. Mech. Eng. Part C J. Mech. Eng. Sci.* **2023**, *237*, 2125–2140. [[CrossRef](#)]

**Disclaimer/Publisher’s Note:** The statements, opinions and data contained in all publications are solely those of the individual author(s) and contributor(s) and not of MDPI and/or the editor(s). MDPI and/or the editor(s) disclaim responsibility for any injury to people or property resulting from any ideas, methods, instructions or products referred to in the content.